NASA TECHNICAL MEMORANDUM

NASA TM X-62,390

NASA TM X-62,390

TECHNIQUES FOR IMPROVING THE STABILITY OF SOFT INPLANE HINGELESS ROTORS

Robert A. Ormiston

Ames Research Center
and
U.S. Army Air Mobility R&D Laboratory
Moffett Field, Calif. 94035

October 1974

TECHNIQUES FOR IMPROVING THE STABILITY OF SOFT INPLANE HINGELESS ROTORS

Robert A. Ormiston

Ames Research Center

and

U. S. Army Air Mobility R&D Laboratory

Moffett Field, CA 94035

SUMMARY

The influence of basic parameters that govern flap-lag stability of hingeless rotor blades in hover is reviewed, and potential methods are studied for improving the lead-lag damping of soft-inplane configurations for low thrust conditions. These conditions are relevant for ground and air resonance stability of coupled rotor-body dynamic systems. Results indicate that the isolated rotor blade lead-lag damping can be usefully increased by a combination of flap-lag elastic coupling and pitch-lag coupling. For a typical soft inplane configuration, 6% of critical damping can be obtained for moderate pitch-lag coupling. For large values of the coupling parameters, the lead-lag frequency is substantially reduced at high pitch angles and airfoil stall effects also reduce the lead-lag damping.

SYMBOLS

a	linear two-dimensional section lift curve slope, rad^{-1}
b	number of blades
c	blade chord, m
c_{d_p}	airfoil profile drag coefficient at zero angle of attack
c_ℓ, c_d	airfoil section lift and drag coefficients
$c_{\ell_o}, c_{d_o}, c_{\ell_\alpha}, c_{d_\alpha}$	nonlinear airfoil section data parameters, local lift and drag coefficients and local lift and drag curve slopes
$C_\beta, C_{\dot{\beta}}, C_\zeta, C_{\dot{\zeta}}, C_{\Delta\theta_a}, C_{\Delta\theta_s}$	coefficients of perturbation lead-lag equation, equation (10)
$F_\beta, F_{\dot{\beta}}, F_\zeta, F_{\dot{\zeta}}, F_{\Delta\theta_a}, F_{\Delta\theta_s}$	coefficients of perturbation flap equation, equation (10)
I	blade inertia, $kg\text{-}m^2$
K	gain parameter, equation (3)
K_β, K_ζ	combined flap and lead-lag spring stiffness at $\theta = 0$, N-m/rad, equation (11)
K_{β_B}, K_{ζ_B}	flap and lead-lag spring stiffness at blade root N-m/rad, figure 20
K_{β_H}, K_{ζ_H}	flap and lead-lag spring stiffness at hub, N-m/rad, figure 20
p	dimensionless rotating flap natural frequency at $\theta_s = 0$, $\sqrt{1 + \bar{w}_\beta^2}$
R	elastic coupling parameter, equation (11) and rotor radius, m
R_w	elastic coupling parameter, equation (11)
R_β, R_ζ	ratios of blade spring flexibility to combined spring flexibility for flap and lead-lag spring restraints, equation (11)

s	Laplace transform variable, sec^{-1}
α	angle of attack, rad
β	blade flapping deflection around a centrally located axis parallel to plane of rotation, rad, figure 20
γ	Lock number, $\rho acR^4/I$
ζ	blade lead-lag deflection around an axis coincident with rotor axis of rotation, rad, figure 20
η_m	lead-lag structural damping parameter
θ	blade pitch angle, rad
θ_s	structural pitch angle, $\theta_{s_o} + \theta$, rad
θ_{s_o}	structural pitch angle at $\theta = 0$ or inclination of principal flexural axes with respect to blade chord line, figure 20
$\theta_\beta, \theta_\zeta$	pitch-flap and pitch-lag coupling parameters
ρ	air density, kg/m^3
σ	rotor solidity, $bc/\pi R$
$\sigma_{\beta,\zeta}$	real part of flap or lead-lag mode eigenvalue, sec^{-1}
ϕ_i	downwash angle at 3/4 blade radius
ω	imaginary part of eigenvalue, rad/sec
$\omega_\zeta, \omega_\beta$	uncoupled lead-lag and flap mode nonrotating natural frequencies in vacuo, $\theta_s = 0$
$\bar{\omega}_\Delta^2$	flap-lag elastic coupling parameter, equation (11)
Ω	rotor angular velocity
$(\,)_o, \Delta(\,)$	steady state and perturbation quantities
$\bar{(\,)}$	nondimensionalized by $R\Omega$ for velocities and Ω for frequencies

INTRODUCTION

The damping of hingeless rotor blade lead-lag motion is inherently small. This is because aerodynamic forces acting on the blade in the lead-lag direction are small and because the mechanical lead-lag dampers of articulated rotors are not usually used on hingeless rotors. The inherently low lead-lag damping, together with the structural properties of cantilever rotor blades, increases the susceptibility of the hingeless rotor to aeroelastic instability, references 1 - 4. Recent investigations, references 4-7, of hingeless rotor aeroelastic stability have provided useful insight about the behavior of these instabilities and in particular about the parameters which stabilize the rotor blade motion by improving the lead-lag damping. The purpose of this report is to study these parameters in detail, specifically to determine ways in which the stability of hingeless rotors might be usefully improved in the hovering flight condition. In particular, primary emphasis is devoted to the soft inplane configurations that are potentially subject to ground and air resonance instability. The analytical methods are based entirely on the rigid hinged blade flap-lag equations of motion developed in references 6 and 8. While these equations only approximate the behavior of an actual hingeless rotor blade, they are sufficiently accurate to describe the general behavior of hingeless rotor blades and will adequately serve the present purpose of investigating means for improving hingeless rotor stability.

BACKGROUND

This section will begin with a brief description of the general stability characteristics of hingeless rotors. This will serve to identify rotor configurations and operating conditions that are most critical in terms of aeroelastic stability. The discussion will also outline some of the basic requirements for rotor stability and suggest a rationale by which these desired characteristics might be achieved.

Hingeless rotor stability analysis can be classified roughly into four distinct areas depending first on whether the system is restricted to isolated rotor blade dynamics or whether the system includes coupled rotor-body dynamics and second on whether the blade lead-lag frequency is greater or less than 1/rev - the stiff and soft inplane configurations respectively.

In general, nearly all helicopter instabilities involve coupled rotor-body dynamics. However, some types of instability involve mainly rotor blade motion dynamics while other types of instability require coupled rotor-body motion. In the first case, the rotor blade stability properties may be modified by rotor-body coupling, but the basic isolated rotor behavior usually remains essentially unchanged. In this case, stable rotor configurations generally will perform satisfactorily when body motion coupling is included. In the second case, where the rotor-body coupling is directly responsible for instability, stability of the isolated rotor may not necessarily prevent a coupled rotor-body instability. Classical ground resonance is an example of this type of instability. This type of instability can be prevented only if the lead-lag damping of the isolated rotor blade is sufficiently increased and this normally requires the addition

of auxiliary mechanical damping. Lead-lag dampers are normally used for conventional articulated rotors and some hingeless rotors, but this solution is undesirable for a number of reasons including weight, reliability, cost, etc.

Soft and stiff inplane hingeless rotors display widely different dynamic behavior in several important respects. First, for the isolated rotor blade condition, the stiff inplane configuration displays more varied and complex behavior than the soft inplane configuration, reference 6. This is consistent with the higher lead-lag bending stiffness for the stiff inplane configuration which increases the structural coupling between bending and torsion deflections. The more complex behavior of the stiff inplane configuration means that there are fewer system parameters that consistently have a favorable or an unfavorable effect on stability. Generally, this makes it more difficult to choose parameters that will increase lead-lag damping independent of other parameter variations. The soft inplane configuration, however, displays a much simpler and consistent behavior. Several parameters can be identified that increase or decrease lead-lag damping in a predictable fashion.

The second difference between the stiff and soft inplane configuration is that for the isolated rotor blade condition, the soft inplane configuration is generally more stable for a wider range of configuration parameters than the stiff inplane configuration, reference 6. That is, for the same range of configuration parameters more cases of instability will be found for stiff inplane than soft inplane rotor blades.

The third important difference between the soft and stiff inplane configurations is that the stiff inplane rotor cannot experience coupled rotor-body mechanical instabilities of the ground resonance type, while the soft inplane configuration can.

In summary, the soft inplane hingeless rotor configuration displays a simpler and more consistent behavior with respect to the influence of system parameters. The soft inplane configuration is also less susceptible to isolated rotor blade instability but more susceptible to coupled rotor-body instability than the stiff inplane configuration. These characteristics of the soft inplane configuration suggest that it may be feasible to identify specific parameters that would increase the lead-lag damping for a stable isolated rotor blade by an amount sufficient to preclude coupled rotor-body instability, without the necessity for auxilliary mechanical lead-lag damping. This general premise forms the basis of this report, and therefore the results will be limited to the soft inplane configuration; although in principle, similar considerations could be applied to the stiff inplane configuration as well. The objective will be to investigate means for increasing rotor blade lead-lag damping by an amount sufficient to prevent the occurrence of a coupled rotor-body instability, primarily ground resonance.

Mechanical instability due to rotor-body coupling may occur whenever the rotor blade lead-lag natural frequency is less then 1/rev and is close to resonance with a body natural frequency (measured in the rotating system). For soft inplane hingeless rotors, these conditions occur both on the ground and in flight and may lead to both ground and air resonance. Whether instability actually occurs depends on several factors, including the coupled rotor-body frequencies, the rotor thrust, and the isolated rotor blade lead-lag damping. The isolated rotor blade lead-lag damping is a function of the rotor thrust. At low thrust levels the damping is mainly due to structural damping of the blade material and the aerodynamic damping from the blade section profile drag. As thrust increases, additional damping is generated due to aerodynamic and inertial coupling between flap and lead-lag bending motions, blade induced

drag due to induced downwash, and torsion motion due to structural coupling between bending and torsion deflections. For certain unfavorable configurations, these effects together may actually reduce damping and the isolated rotor blade may be unstable. Such configurations will not be considered in this report.

Soft inplane hingeless rotor helicopters will be free from ground and air resonance instability if the combined structural and aerodynamic damping of the blades is sufficiently high or if the auxilliary mechanical lead-lag dampers are provided. The most critical condition, however, is generally the low thrust condetion when the blade lead-lag damping is a minimum. Therefore, ground resonance instability, at zero or low thrust is generally the critical operating condition. Air resonance would generally be less critical since the rotor is operating at moderately high thrust for most flight conditions. An exception would be flight at zero "g" load factor; although this would probably occur only during rapid or transient maneuvering conditions. The effect of thrust on ground and air resonance stability noted here does not consider the effects of changes in the coupled rotor-body frequencies for different flight conditions. This discussion applies only to the influence of rotor thrust on the isolated blade lead-lag damping.

Since the minimum isolated rotor blade lead-lag damping occurs at zero or low rotor thrust, this operating condition will be emphasized in this report. Methods of increasing the damping at zero thrust could adversely influence the damping at high thrust conditions or adversely influence other rotor characteristics and this will also be investigated. It is assumed that the influence of rotor-body coupling on the increment of isolated blade lead-lag damping produced by a favorable choice of configuration parameters will be small. It is beyond the scope of this report to prove the accuracy of this assumption and this must be considered in assessing the present results.

HINGELESS ROTOR STABILITY CHARACTERISTICS

Previous investigations of flap-lag stability of isolated (without rotor-body coupling) hingeless rotor blades in hover have described the general stability behavior and identified several parameters that would favorably influence stability by increasing the lead-lag damping, e.g., reference 6. The analyses were based on a centrally hinged, spring restrained, rigid blade, representation of an elastic blade that neglected torsional blade deflections. This approximate representation has been shown to be reasonably accurate for typical rotor blade configurations when appropriate pitch-flap and pitch-lag coupling factors are introduced to account for the effects of torsion deflections, reference 7. This type of analysis will be used in this report and the linearized equations for the hovering flight condition are given in the appendix.

Two important factors that influence the stability of soft inplane hingeless rotor blades are pitch-lag coupling and structural or elastic coupling of the flap and lead-lag deflections. Figure 1 shows the effect of flap-lag elastic coupling on the eigenvalues of a typical soft inplane configuration. This basic configuration will be used throughout the report. The lead-lag frequency is 0.7Ω, the flap frequency is 1.1Ω, and the Lock number is 8.0. The values of R represent the degree of elastic coupling. For R = 0 the flap and lead-lag deflections are uncoupled for all blade pitch angles. For R = 1, the deflections are fully coupled and the coupling is proportional to pitch angle (at small angles). At zero pitch angle the lead-lag damping is very small (due to blade section profile drag) and without elastic coupling it increases only

slightly as pitch angle increases. The increase is due to aerodynamic and inertial flap-lag coupling as well as the induced drag damping. For configurations with flap-lag elastic coupling, the lead-lag mode is further stabilized as the weakly damped lead-lag mode becomes more strongly coupled with the highly damped flap mode.

The effect of pitch-lag coupling is shown in figure 2 for the same soft inplane configuration and for R = 1.0. Pitch-lag coupling introduces a strong aerodynamic coupling between the flap and lead-lag deflections that is strongly stabilizing as the blade pitch angle is increased. At zero pitch angle, there is no increase in damping. At high pitch angles, large values of pitch-lag coupling also produce large reductions in the blade lead-lag frequency.

The results of figures 1 and 2 show that lead-lag damping may be substantially increased by flap-lag elastic coupling and pitch-lag coupling, and that the effectiveness of these couplings increases as the blade pitch angle is increased. By properly choosing the structural properties in bending and torsion, the effective elastic pitch-lag coupling can substantially improve lead-lag damping when the rotor operates at normal thrust conditions, reference 5. For small values of rotor thrust, the flap-lag elastic coupling and pitch-lag coupling do not increase lead-lag damping, however, and these methods are ineffective. The next section will describe other techniques that may be used to increase lead-lag damping for low thrust conditions.

TECHNIQUES FOR INCREASING LEAD-LAG DAMPING AT LOW THRUST

Consider first the structural or elastic coupling between flap and lead-lag bending deflections. The coupling term, taken from the equations in the appendix, is

$$\frac{R\bar{\omega}_{\Delta}^{2}}{2\Delta} \sin 2\theta_{s} \qquad (1)$$

where $\bar{\omega}_{\Delta}^{2} = \bar{\omega}_{\zeta}^{2} - \bar{\omega}_{\beta}^{2}$ is the difference between the lead-lag and flap bending stiffnesses of the blade and where θ_{s} is the pitch angle of the major principal flexural axis of the blade cross section. For typical rotor blade structures, this principal axis nearly coincides with the chord line (angle of zero lift) of the blade airfoil section. Therefore, the structural pitch angle of the blade is approximately equal to the [aerodynamic] pitch angle of the blade, $\theta_{s} \approx \theta$. In this case, the flap-lag elastic coupling provides no significant increase in lead-lag damping at zero pitch angle. This coupling could be provided at zero pitch angle if the blade structure were designed so that the major principal flexural axis did not coincide with the blade airfoil chord line. The effect of such a change is shown in figure 3, where θ_{s_o} is equal to the angle between the major principal flexural axis of the blade cross section and the airfoil chord line (Note that $\theta_{s} = \theta_{s_o} + \theta$). For these results R = 1.0. The results of figure 3 show a small increase in damping at zero pitch angle for moderately large values of θ_{s_o}. Although the damping increased by a factor of five, the absolute value remains low, and is only slightly more than 1% of critical damping. The substantial

change in frequency is due to the effective reduction in lead-lag stiffness as the orientation of the principal flexural axes is changed.

Introducing pitch-lag coupling in combination with the above flap-lag elastic coupling ($\theta_{s_o} > 0$) is considerably more effective in producing increased lead-lag damping at zero blade pitch angle. Figure 4 shows the eigenvalues again for R = 1.0 and $\theta_{s_o} = 36°$ for several values of pitch-lag coupling. The lead-lag damping at zero pitch angle is substantially increased but in comparison with figure 3 the damping at high pitch angles is slightly reduced. The frequency reduction with pitch angle noted in figure 3 is magnified by pitch-lag coupling in figure 4.

The role of the various coupling factors can be clearly summarized by plotting the real part of the lead-lag mode eigenvalue as a function of pitch angle. Figure 5 again shows that, although pitch-lag coupling is very effective for increasing lead-lag damping at pitch angles greater than zero, a combination of θ_ζ and θ_{s_o} is required to produce a significant increase in lead-lag damping at zero pitch angle. For $\theta_{s_o} = 36°$ and $\theta_\zeta = -.5$ the lead-lag damping is greater than 6% of critical damping at zero pitch angle.

A relatively simple explanation of effectiveness of the combination of couplings noted above may be obtained by examining the flap-lag equations of motion for the zero pitch angle condition. The effect of pitch-lag coupling is included by substituting the relation $\Delta\theta = \theta_\zeta \Delta\zeta$ into the perturbation equations given in the appendix. The small contribution of β_o at $\theta = 0$ can be neglected.

$$\begin{bmatrix} s^2 + \frac{\gamma}{8} s + 1 + \frac{1}{\Delta}\left[\bar{\omega}_\beta^2 + R\bar{\omega}_\Delta^2 \sin^2 \theta_{s_o}\right] & \frac{R\bar{\omega}_\Delta^2}{2\Delta} \sin 2\theta_{s_o} - \frac{\gamma}{8}\theta_\zeta \\ \frac{R}{2}\frac{\bar{\omega}_\Delta^2}{\Delta} \sin 2\theta_{s_o} & s^2 + \frac{\gamma}{8}\left(\frac{2c_{d_o}}{a}\right)s + \frac{1}{\Delta}\left[\bar{\omega}_\zeta^2 - R\bar{\omega}_\Delta^2 \sin^2 \theta_{s_o}\right] \end{bmatrix} \begin{Bmatrix} \Delta\beta \\ \Delta\zeta \end{Bmatrix} = 0 \qquad (2)$$

The structural coupling, afforded by inclining the principal flexural axes appears as antisymmetric terms in the matrix, whereas, the pitch-lag coupling term appears as a non-antisymmetric coupling term. Without the coupling terms, the eigenvalues are given simply by the uncoupled flap and lead-lag equations. In the latter, the damping is $\frac{\gamma}{8}\frac{c_{d_o}}{a}$. When the coupling terms are stabilizing, their influence is governed by the product defined by

$$K \equiv \frac{R}{2}\frac{\bar{\omega}_\Delta^2}{\Delta}\sin 2\theta_{s_o}\left(\frac{R}{2}\frac{\bar{\omega}_\Delta^2}{\Delta}\sin 2\theta_{s_o} - \frac{\gamma}{8}\theta_\zeta\right) \tag{3}$$

In the case where θ_ζ is zero, K has a relatively small value proportional to $\sin^2 2\theta_{s_o}$. For the case when θ_{s_o} (or R or $\bar{\omega}_\Delta^2$) equals zero, K = 0 and pitch-lag coupling can have no effect on the lead-lag damping. Only when both θ_{s_o} and θ_ζ are nonzero can K have an appreciably large value. This explains why θ_{s_o} alone has a small influence on lead-lag damping at $\theta = 0$, and θ_ζ alone has no influence. For soft inplane configurations, θ_ζ must be negative to improve lead-lag damping, i.e. the blade pitch must decrease for lead bending and increase for lag bending.

The relation for K also shows how the effectiveness of the coupling terms varies with R, $\bar{\omega}_\Delta^2$, and γ. As noted in the appendix, the equations are valid for configurations where only the blade principal flexural axes are inclined at the angle θ_{s_o} with respect to the chord line. The hub flexural axes (inboard of the pitch bearing) remain at zero pitch angle. In this case the flap-lag elastic coupling for a pitch angle $\theta = 0$ will be maximum when R = 1.0, that is when all bending flexibility is allocated to the blade outboard of the pitch bearing. For the present report, R is chosen to be 1.0 for convenience and this also represents a typical configuration. The

parameter K also depends on the difference in bending stiffnesses $\bar{\omega}_\Delta^2$. For a matched stiffness configuration $\bar{\omega}_\Delta^2 = 0$ and no benefit will result from the coupling effects being discussed. Finally, the blade Lock number γ directly multiplies the effectiveness of pitch-lag coupling.

EFFECT OF BASIC SYSTEM PARAMETERS

At zero pitch angle the increase in lead-lag damping depends on the product of the coupling terms K and the basic system parameters of the uncoupled equations p, $\bar{\omega}_\zeta$, and γ. Since these parameters also influence the coupling terms in K, it is useful to consider the effect of K on lead-lag damping for typical values of the basic system parameters independent of the effect of those parameters on K itself. The variation of the eigenvalues of the flap-lag equations at zero pitch angle can be obtained by standard root locus techniques using K as the gain parameter. The characteristic equation, in root locus form is given by

$$1 - \frac{K}{\left(s^2 + \frac{\gamma}{8}s + p^2\right)\left(s^2 + \frac{\gamma}{8}\left(\frac{2c_{d_p}}{a}\right)s + \bar{\omega}_\zeta^2\right)} = 0 \qquad (4)$$

where p and $\bar{\omega}_\zeta$ are the uncoupled dimensionless flap and lead-lag frequencies, respectively. These may be modified to include the effects of θ_{s_o} included in equation (2) but for the present purposes this is not significant.

For typical values of the basic system parameters, p = 1.1, $\bar{\omega}_\zeta = 0.7$, $\gamma = 8$, and $c_{d_p} = 0.01$, the root locus for varying K is given in figure 6

for positive and negative values of K. The range of K is much larger than would be found on a typical rotor blade, but this illustrates the asymptotic behavior of the root locus. Typical values for K would normally be less than 0.1 to 0.2 for a soft inplane rotor blade with large pitch-lag coupling. Figure 6 shows that positive values of K are stabilizing for the lead-lag mode and that negative values are destabilizing. Significant variations in frequency also occur. For the flap mode, the frequency variations are smaller for small values of K, and the variations in damping are not as significant.

Increasing the flap frequency p has a significant effect on the lead-lag mode root locus; decreasing the damping and increasing the frequency for positive K as shown in figure 7. This illustrates that as the poles of the root locus (the uncoupled frequencies p and $\bar{\omega}_\zeta$) move together the sensitivity of the root locus to the coupling parameter K is increased. The maximum increase in lead-lag damping would, therefore, be expected when $p \simeq \bar{\omega}_\zeta$. This is clearly evident from the root loci in figure 8 for various values of lead-lag frequency $\bar{\omega}_\zeta$. Finally, figure 9 shows root loci for various values of Lock number γ. These results again indicate that the proximity of the lead-lag and flap frequencies is the predominant factor for lead-lag damping. In the limit as $\gamma \to 0$ the damping would be zero for practical values of K.

Lead-lag mode frequency and damping as a function of K for the typical soft inplane configuration are given in figure 10. Equation (3) for K may be used with this figure to estimate frequency and damping for various values of θ_{s_o} and θ_ζ. The sensitivity of the lead-lag damping to the basic system parameters is given in figure 11 for a value of K = 0.1.

EFFECTS OF COUPLING PARAMETERS ON FLAP-LAG DYNAMICS

The preceding sections have described techniques that may be used to improve the stability of soft inplane hingeless rotor blades at zero pitch angle. The simplified flap-lag equations and root loci illustrated the effectiveness of a combination of pitch-lag coupling and flap-lag elastic coupling and the senstitivity of rotor blade stability to basic system parameters. In this section a broader and more detailed investigation of the coupling parameters, including pitch-flap coupling, will be undertaken, including the influence of θ_{s_o} on the coupled blade natural frequencies and the effects of airfoil stall at high pitch angles.

Blade Natural Frequencies

For the results presented above, the favorable effects of flap-lag elastic coupling were proportional to the difference between the nonrotating lead-lag and flap frequencies, $\bar{\omega}_\Delta^2 = \bar{\omega}_\zeta^2 - \bar{\omega}_\beta^2$, and the inclination of the major principal flexural axis θ_{s_o}. This means that for maximum lead-lag damping the inplane frequency should be high, the nonrotating flap frequency should be low, and θ_{s_o} should be large. The lead-lag frequency of soft inplane rotors is constrained from resonance with the 1/rev blade rotational frequency which limits its maximum value to roughly 0.7 - 0.8/rev or lower depending on the configuration. The flexural axis inclination θ_{s_o} is limited only by fabrication techniques. The maximum value for $\sin 2\theta_{s_o}$ occurs when $\theta_{s_o} = 45°$. For high values of θ_{s_o}, the rotating lead-lag natural frequency is reduced below $\bar{\omega}_\zeta$ and it becomes a relatively strong function of blade pitch angle. A large reduction in the lead-lag natural frequency would be detrimental for ground resonance stability since the lead-lag damping required to prevent ground resonance varies roughly inversely with the lead-lag frequency.

The nonrotating flap frequency $\bar{\omega}_\beta$ is typically small and should be minimized to increase $\bar{\omega}_\Delta{}^2$. Generally, however, $\bar{\omega}_\beta$ is constrained by other design considerations and there is little opportunity to influence lead-lag stability.

The lead-lag natural frequencies, in vacuo, through a 90° range of θ_{s_o} are given in figures 12(a) and 12(b) for $\bar{\omega}_\zeta = 0.5$ and 0.7, respectively. Several typical values of flap frequency p are included where $p = \sqrt{1 + \bar{\omega}_\beta{}^2}$. For $\bar{\omega}_\zeta = 0.5$ and a representative value of $\theta_{s_o} = 36°$, only relatively small changes in frequency are found. For $\bar{\omega}_\zeta = 0.7$, which provides a greater increase in lead-lag damping, the lead-lag natural frequency is substantially reduced at $\theta_{s_o} = 36°$. Higher values of $\bar{\omega}_\zeta$ to raise the lead-lag natural frequency might be feasible since the problem of 1/rev resonance is postponed by the effect of θ_{s_o}. The flap natural frequencies are also influenced by θ_{s_o} for $\bar{\omega}_\zeta = 0.7$ and this may be significant since the control response and flying qualities of the hingeless rotor are quite sensitive to the flap frequency. For the example configuration used in this report $\bar{\omega}_\zeta = 0.7$, $p = 1.1$ (at $\theta_{s_o} = 0°$), the natural frequencies at $\theta_{s_o} = 36°$ are .635 and 1.157, respectively. This flap frequency is within the range of values found for typical rotor blades; however, further increases would be detrimental to control response and flying qualities.

Flap-Lag Elastic Coupling, $\theta = 0°$

The structural coupling between flap and lead-lag bending is maximum at 45° and it would be expected that its effect on lead-lag damping would be largest for values of $\theta_{s_o} \simeq 45°$. Figures 13(a) and 13(b) show this to be the case for both pitch-lag and pitch-flap coupling. The angle for maximum damping is usually slightly less than 45° and for most of the results in this report a nominal value of $\theta_{s_o} = 36°$ is chosen. These figures further illustrate that when $\sin 2\theta_{s_o} = 0$ the lead-lag damping is not influenced by pitch-lag or pitch-flap coupling.

Pitch-Lag and Pitch-Flap Coupling, $\theta = 0$

The simplified discussion of the equations given above did not treat pitch-flap coupling. Pitch-flap coupling mainly influences the uncoupled flap frequency. Pitch-flap coupling also contributes to the flap coupling term in the lead-lag equation but the magnitude of this term (since it is multiplied by the inflow angle ϕ_i) is much smaller than the corresponding pitch-lag coupling term in the flap equation. At zero pitch angle, where $\phi_i = 0$, pitch-lag coupling influences only the uncoupled flap frequency and pitch-lag coupling influences only the coupling term in the flap equation. There is no effect of these couplings on the lead-lag equation.

Since pitch-flap coupling influences the flap frequency, its effect on lead-lag damping would be expected to follow the trends noted above for flap frequency variations. Positive values of θ_β, which increase the flap frequency, will reduce the lead-lag damping because of the increased separation between the flap and lead-lag frequencies. Negative values of θ_β will have the opposite effect. Therefore, θ_β can be thought of as a measure of the flap frequency p, a basic system parameter, whereas, θ_ζ and θ_{s_o} can be thought of as influencing the coupling parameter K. The uncoupled flap frequency, including the effect of θ_β, is

$$\frac{\omega}{\Omega} = p^2 - \frac{\gamma}{8}\theta_\beta \tag{5}$$

where the small contribution of θ_{s_o} is neglected.

The combined effects of pitch-flap and pitch-lag coupling on lead-lag damping of the typical soft inplane configuration at zero pitch angle and $\theta_{s_o} = 36°$ are shown in figures 14(a) and 14(b). In figure 14(a) the damping is given as a

function of θ_ζ for a series of values of θ_β. Variations in θ_β serve to alter the sensitivity of the lead-lag damping to pitch-lag coupling, as the effective flap frequency is changed. Positive values of θ_β increase the sensitivitiy of the damping to pitch-lag coupling and negative values decrease the sensitivity. The lead-lag damping may be alternately considered as a function of θ_β for various values of pitch-lag coupling, as shown in figure 14(b). Here, for zero pitch-lag coupling, the variation in lead-lag damping with θ_β is small because only the contribution of flap-lag elastic coupling from θ_{s_o} is present. For non-zero values of pitch-lag coupling, the damping is greatly increased. The largest effect occurs when $\theta_\beta \simeq .8$ because the flap frequency is reduced nearly equal to the lead-lag frequency. The locus of roots of the flap and lead-lag eigenvalues, with θ_β varying, is shown in figure 15. The coalescence of frequencies is clearly seen. For large values of pitch-lag coupling, and intermediate values of θ_β, the flap and lead-lag modes become strongly coupled and lose their separate identity.

Pitch-flap coupling is of practical significance with respect to techniques for improving the stability of hingeless rotors. Generally, however, conflicting requirements for pitch-flap coupling can be expected to have an adverse effect on lead-lag damping because of certain constraints on θ_β determined by hingeless rotor flying qualities. Negative pitch-flap coupling is commonly employed on hingeless rotors to minimize adverse flapping response sensitivity at high flight speeds by increasing the flap frequency. Unfortunately, this is opposite the desired pitch-flap coupling for improving lead-lag damping. Other techniques are available for reducing flapping response sensitivity; however, it is unlikely that any significant positive values of pitch-flap coupling could be tolerated for the purposes of improving lead-lag damping.

Lead-Lag Frequency and Damping, $\theta > 0$

This report is concerned mainly with techniques for improving hingeless rotor blade stability at zero blade pitch angle. However, dynamic characteristics at normal operating pitch angles must not be adversely degraded by these techniques. Results discussed above, figure 5, showed that for $\theta_\zeta = -.5$ the lead-lag damping at high pitch angles was reduced with the addition of flap-lag elastic coupling for $\theta_{s_o} = 36°$. At high pitch angles, the lead-lag damping is also very large and this reduction is not significant.

The variation of lead-lag frequency at high pitch angles is more significant however. Figure 16 shows the variation of lead-lag frequency with pitch angle for several values of pitch-lag coupling with $\theta_{s_o} = 36°$. For low values of pitch-lag coupling, the reduction in frequency with increased pitch angle is not large, but for large values of pitch-lag coupling the reduction in frequency is large. This may be of concern in regard to the vibratory response of lead-lag bending to periodic aerodynamic excitation in forward flight. Although the response would not necessarily be increased as the frequency was reduced, the variation in frequency with pitch angle (and hence, different flight conditions) would make it more difficult to tune the fuselage structure to minimize dynamic response to blade forces.

Typical Values for Lead-Lag Damping

The probable benefit of applying the techniques outlined in this report will depend on the values chosen for the basic system parameters $\bar{\omega}_\zeta$, p, γ, and the coupling parameters θ_ζ and θ_{s_o}. It is useful to examine the lead-lag damping of a soft inplane hingeless rotor for two different cases, based on both the

favorable and unfavorable extremes of the variations in typical parameter values. This will illustrate the range of damping values that might be expected. Figure 17a shows results for the configuration with favorable values ($p = 1.1$, $\bar{\omega}_\zeta = 0.7$, $\gamma = 8$) as a function of pitch-lag coupling for several values of θ_{s_o}. The lead-lag damping is given in terms of percent critical damping, or 100 times the lead-lag mode damping ratio ζ. In terms of the real and imaginary components of the eigenvalue, the damping ratio is given by

$$\zeta = \frac{\sigma/\Omega}{\sqrt{\left(\frac{\sigma}{\Omega}\right)^2 + \left(\frac{\omega}{\Omega}\right)^2}} \tag{6}$$

For $\theta_{s_o} = 36°$ the damping is over 11% at $\theta_\zeta = -1.0$ and over 6% at $\theta_\zeta = -.5$.

With unfavorable parameter values ($p = 1.15$, $\bar{\omega}_\zeta = 0.6$, $\gamma = 5$) the maximum damping is reduced by more than an order of magnitude as shown in figure 17b. These low values would be of no significant benefit and illustrate that the basic system parameters must be carefully chosen to obtain useful increases in the lead-lag damping.

Effects of Airfoil Stall at Large Blade Pitch Angles

The effects of airfoil stall are known to strongly influence hingeless rotor stability at high blade pitch angles and may cause instability for otherwise stable configurations, reference 8. The analysis of reference 8 includes only the quasi-static effects of stall on the airfoil lift and drag. Unsteady aerodynamics and stalled pitching moment effects would be expected to further influence stability of torsionally flexible hingeless rotor configurations. These effects would greatly complicate the analysis, however, and are not

considered here. The main purpose of this section is to briefly examine some of the gross effects of stall on flap-lag stability when various coupling parameters are included. The results of reference 8 showed that for the soft inplane configuration, the lead-lag damping was increased by airfoil stall and the flap damping was decreased by stall. With flap-lag elastic coupling θ_{s_o} and pitch-lag coupling θ_ζ included, the effects of stall are not greatly changed as shown in figures 19 and 20. The same low Reynolds number airfoil lift and drag curves that were used in reference 8 were used for the present results.

$$c_\ell = 2\pi\alpha - 10\alpha^2$$
$$c_d = c_{d_p} + 11.1\alpha^3 \qquad (7)$$

These airfoil characteristics are highly conservative compared to normal airfoils at typical full scale Reynolds numbers, but they do serve to clearly illustrate the trends that can be expected.

Figure 18, without flap-lag elastic coupling ($\theta_{s_o} = 0$) shows the effect of stall for various values of pitch-lag coupling. This locus of roots may be compared with figure 2 without stall. For $\theta_\zeta = 0$, stall stabilizes the lead-lag mode and causes instability for the flap mode. For non-zero values of θ_ζ, the lead-lag damping is decreased. With the addition of flap-lag elastic coupling ($\theta_{s_o} = 36°$) there is a further reduction in lead-lag damping at high pitch angles, figure 19. The reduction in lead-lag frequency is also greater. While the effects of stall do not improve the rotor blade stability it may be noted as above that very conservative airfoil stall characteristics have been used and that the flap mode instability occurs only at very high pitch angles, usually well beyond those for typical rotor operating conditions.

ADDITIONAL CONSIDERATIONS

The scope of this report is limited to the stability characteristics of an isolated hingeless rotor blade with flap and lead-lag bending degrees of freedom. The results are intended to indicate how the isolated rotor blade damping may be improved in order to prevent more complex, coupled, rotor-body instabilities such as ground and air resonance. The purpose of this section is to examine the significance of several of the limitations and simplifying assumptions of the present report and to discuss the probable impact of eliminating them. We will consider the effects of blade torsion, rotor-body coupling, and unsteady downwash dynamics.

The effects of blade torsion could be included in the present isolated blade analysis, but the basic results would not be changed significantly. Except for special blade configurations with very low torsion frequencies, only the structural effects of torsion need to be considered and these can be satisfactorily represented by variations in the pitch-lag and pitch-flap coupling parameters. For simple rotor hub configurations, without significant precone or sweep of the blade, the effective pitch-lag and pitch-flap couplings due to blade torsion will be negligible at low rotor thrust. Therefore most of the results of this report are essentially unaffected by torsional deflections of the blade. For nonzero values of rotor thrust, the associated coning of the blades will produce a significant effective pitch-lag coupling due to torsion. This coupling is negative and will increase the lead-lag damping for soft inplane blades as the rotor thrust increases above zero. In

the case of soft inplane configurations with positive precone, somewhat different behavior would be expected. At zero rotor thrust, the blades would deflect below the static preconed position introducing an effective positive pitch-lag coupling that would destabilize the rotor blade. However, the increments in lead-lag damping obtainable with the techniques of this report would be essentially independent of the effects of precone.

It has been assumed that the improvements in isolated blade damping described in this report would also be realized when coupling between the rotor and body was present. This is based on the rationale that the requirements for prevention of ground and air resonance are often specified in terms of a specific value of auxilliary mechanical lead-lag damping. It has been assumed here that this would hold true if the incremental damping was obtained aerodynamically by altering the coupled flap-lag dynamics of the blade. In other words, an increment of lead-lag damping is assumed to be equally effective in preventing ground or air resonance, independent of whether it is mechanical or aerodynamic in origin. Implicit in this assumption are two factors which must be considered in more detail. The first is the direct effect of rotor-body coupling dynamics on the favorable increment of aerodynamic lead-lag damping (of the isolated blade), and the second is the indirect effect of the unsteady downwash dynamics which may further influence the rotor-body coupling.

In the first case, it is expected that the direct effect of rotor-body coupling will not be quantitatively significant and that the aerodynamic increments in lead-lag damping due to favorable coupling effects discussed in this report may be considered equivalent to auxilliary mechanical lead-lag damping.

The effects of the rotor wake induced downwash may be more significant, however, particularly for the low thrust hover condition of interest. This is because the effects of rotor downwash are more significant for ground and air resonance of hingeless rotors than for articulated rotors. The main reason for this difference is the influence of the large value of angular rate damping of the hingeless rotor. Usually, the ground or air resonance mode involves a coupling of blade lead-lag motion with horizontal translatory motion of the rotor hub. Translatory motion of the rotor hub also produces angular motion of the helicopter body which introduces the effects of angular rate damping of the rotor. The large angular rate damping of the hingeless rotor acts as a stabilizing influence for ground or air resonance. The significance of the wake induced downwash is that at low rotor thrust beneficial influence of angular rate damping can be substantially reduced. The reason for this is that hub moments (including damping moments) of the hingeless rotor generate large azimuthwise nonuniformities in the induced downwash that modify the distribution of rotor lift forces and in turn reduce the original hub moment. The nonuniformities in downwash vary roughly inversely with rotor thrust and thus the hub moment response at low thrust is greatly reduced, reference 9. The reduction in the steady state hub moment response can also be considered as an effective reduction in the rotor blade flapping, damping or the Lock number. For unsteady conditions, the dynamic response of the downwash to rotor hub moments is also important, and this effect counteracts to some extent the reduction in hub moment response or blade flap damping, reference 10.

The effects of hingeless rotor downwash may, therefore, have a specific effect on the favorable increments of isolated rotor blade lead-lag damping. These increments of damping are generated aerodynamically by coupling between

the flap and lead-lag motions of the blade. In effect, the weakly damped lead-lag mode is stabilized by the heavily damped flap mode. If the influence of nonuniform downwash is to effectively reduce the flap mode damping of the rotor blade then there may be an unfavorable influence on the aerodynamic increments of lead-lag damping at low thrust. It is not possible to accurately estimate the adverse effects of rotor downwash and rotor-body coupling because of the complexity of the phenomena involved. This will depend on the coupled rotor-body modes shapes, the frequencies, details of the downwash aerodynamics, blade twist effects, and other factors.

CONCLUSIONS

1. Useful improvements in the stability of isolated soft inplane hingeless rotor blades may be obtained for the low thrust hover flight condition by incorporating a suitable combination of elastic flap-lag coupling and pitch-lag coupling. For favorable typical values of Lock number and bending stiffnesses, up to 6% critical damping of the lead-lag mode may be achieved for a pitch-lag coupling of -0.5. For unfavorable parameter values, however, the improvements in lead-lag damping will be very small.

2. The flap-lag elastic coupling and pitch-lag coupling are effective in improving lead-lag damping at zero pitch angle when they are used together in combination. Flap-lag elastic coupling alone provides only a small increase in damping and pitch-lag coupling alone provides no increase in damping at zero pitch angle. The effects of this combination of couplings are increased when the difference between the uncoupled flap and lead-lag natural frequencies is reduced.

3. In the range of typical soft inplane rotor configuration parameter values, lead-lag damping is increased as Lock number is increased, as flap frequency is reduced, and as lead-lag frequency is increased.

4. Pitch-flap coupling has a significant effect on lead-lag damping primarily because of its influence on the uncoupled flap frequency. Lead-lag damping is increased for positive values of θ_β. Positive values of θ_β also produce a detrimental increase in rotor flapping sensitivity and, therefore, pitch-flap coupling is not a practical means for improving soft inplane hingeless rotor stability.

5. Large values of flap-lag elastic coupling and pitch-lag coupling cause significant reductions in the lead-lag frequency at high pitch angles. Restrictions

on the minimum lead-lag frequency may influence the maximum practical lead-lag damping that can be obtained.

6. When flap-lag elastic coupling and pitch-lag coupling are included, airfoil stall reduces lead-lag damping at high pitch angles compared to configurations without such couplings. Except for extreme pitch angles, the lead-lag damping remains higher than the damping without stall. The coupling parameters do not substantially influence the flap mode instability of soft inplane configurations in the stall condition.

7. The improvements in hingeless rotor blade stability described in this report are intended to alleviate ground and air resonance problems for soft inplane hingeless rotorcraft. It should be noted, however, that the coupling parameters improve the rotor blade lead-lag damping aerodynamically and that additional coupling between the rotor-body may also influence these improvements. For example, at low thrust level, the effective blade Lock number is reduced due to unsteady nonuniform downwash. The present results apply only to the isolated rotor blade condition and do not reflect the additional effects of rotor-body coupling.

REFERENCES

1. Johnston, J. F., and Cook, J. R., "AH-56A Vehicle Development" Paper presented at the 27th Annual National Forum of the American Helicopter Society, Preprint No. 574, Washington D. C., May, 1971.

2. Donham, R. E.; Cardinale, S. V.; and Sachs, I. B., "Ground and Air Resonance Characteristics of a Soft Inplane Rigid-Rotor System," Journal of the American Helicopter Society, Vol. 14, No. 4, October, 1969.

3. Anderson, W. D., "Investigation of Reactionless Mode Stability Characteristics of a Stiff Inplane Hingeless Rotor System " Preprint No. 734, presented at the 29th Annual National Forum of the American Helicopter Society, Washington, D. C., May, 1973.

4. Lytwyn, R. T.; Miao, W.; and Woitch, W., "Airborne and Ground Resonance of Hingeless Rotors," Preprint No. 414. Paper presented at the 26th Annual National Forum of the American Helicopter Society, Washington, D. C., June, 1970.

5. Huber, H. B., "Effect of Torsion-Flap-Lag Coupling of Hingeless Rotor Stability," Preprint No. 731, Paper presented at the 29th Annual National Forum of the American Helicopter Society, Washington, D., C., May, 1973.

6. Ormiston, R. A., and Hodges, D. H., "Linear Flap-Lag Dynamics of Hingeless Helicopter Rotor Blades in Hover," Journal of the American Helicopter Society, Vol. 17, No. 2, April, 1972.

7. Hodges, D. H., and Ormiston, R. A., "Stability of Elastic Bending and Torsion of Uniform Cantilevered Rotor Blades in Hover," Paper No. 73-405, presented at the AIAA/ASME/SAE 14th Structures, Structural Dynamics, and Materials Conference, Williamsburg, Virginia, March, 1973.

8. Ormiston, R. A., and Bousman, W. G., "A Study of Stall-Induced Flap-Lag Instability of Hingeless Rotors," Paper presented at the 29th Annual National Forum of the American Helicopter Society, Preprint No. 730, Washington, D. C., May, 1973.

9. Ormiston, R. A., and Peters, D. A., "Hingeless Helicopter Rotor Response with Nonuniform Inflow and Elastic Blade Bending," Journal of Aircraft, Vol. 9, No. 10, October, 1972.

10. Peters, D. A., "Hingeless Rotor Frequency Response with Unsteady Inflow," Proceedings AHS/NASA-Ames Specialists' Meeting on Rotorcraft Dynamics, Paper No. 1, NASA SP-352, Moffett Field, California, February, 1974.

APPENDIX

Flap-Lag Equations

The equations of motion for the flap and lead-lag deflections of a centrally hinged, spring restrained, rigid blade, rotating at constant angular velocity, around a fixed hub are taken from the derivations of references 6 and 8. The blade deflections, and restraint springs are shown in figure 20. The equations are linearized about the equilibrium flap and lead-lag deflections and are based on quasi-steady strip theory aerodynamics, including stall.

Equilibrium Equations

$$\begin{bmatrix} F_\beta & F_\zeta \\ C_\beta & C_\zeta \end{bmatrix} \begin{Bmatrix} \beta_o \\ \zeta_o \end{Bmatrix} = \begin{Bmatrix} F_\theta \\ C_\theta \end{Bmatrix} \theta \tag{8}$$

Perturbation Equations

$$\begin{bmatrix} s^2 + F_\beta^\bullet s + F_\beta & F_\zeta^\bullet s + F_\zeta \\ C_\beta^\bullet s + C_\beta & s^2 + C_\zeta^\bullet s + C_\zeta \end{bmatrix} \begin{Bmatrix} \Delta\beta \\ \Delta\zeta \end{Bmatrix} = \begin{Bmatrix} F_{\Delta\theta_a} \\ C_{\Delta\theta_a} \end{Bmatrix} \Delta\theta + \begin{Bmatrix} F_{\Delta\theta_s} \\ C_{\Delta\theta_s} \end{Bmatrix} \Delta\theta \tag{9}$$

where

$$\left.\begin{aligned}
F_\beta^\bullet &= -\frac{\gamma}{8a}\left[\phi_i\, c_{d_\alpha} - c_{\ell_\alpha} - c_{d_o}\right] \\
F_\zeta^\bullet &= -\frac{\gamma}{8a}\left[2c_{\ell_o} + \phi_i\left(c_{\ell_\alpha} - \phi_i c_{d_\alpha} - c_{d_o}\right)\right] + 2\beta_o \\
C_\beta^\bullet &= \frac{\gamma}{8a}\left[c_{\ell_o} - \phi_i c_{\ell_\alpha} - c_{d_\alpha}\right] - 2\beta_o \\
C_\zeta^\bullet &= \frac{\gamma}{8a}\left[2c_{d_o} + \phi_i\left(c_{\ell_o} + c_{d_\alpha} + \phi_i c_{\ell_\alpha}\right)\right] + 2\eta_m\bar{\omega}_\zeta \\
F_{\Delta\theta_a} &= \frac{\gamma}{8a}\left[c_{\ell_\alpha} - \phi_i c_{d_\alpha}\right] \\
C_{\Delta\theta_a} &= -\frac{\gamma}{8a}\left[c_{d_\alpha} + \phi_i c_{\ell_\alpha}\right]
\end{aligned}\right\} \tag{10}$$

Continued

$$
\left.
\begin{aligned}
F_\theta &= \frac{\gamma}{8a}\left[c_{\ell_o} - \phi_i c_{d_o}\right] \\
C_\theta &= -\frac{\gamma}{8a}\left[c_{d_o} - \phi_i c_{\ell_o}\right] \\
F_\beta &= 1 + \frac{1}{\Delta}\left[\bar{\omega}_\beta^{2} + R\bar{\omega}_\Delta^{2}\sin 2\theta_s\right] \\
F_\zeta &= C_\beta = \frac{R\bar{\omega}_\Delta^{2}}{2\Delta}\sin 2\theta_s \\
C_\zeta &= \frac{1}{\Delta}\left[\bar{\omega}_\zeta^{2} - R\bar{\omega}_\Delta^{2}\sin^2\theta_s\right] \\
F_{\Delta\theta_s} &= \frac{R\bar{\omega}_\Delta^{2}}{\Delta}\left[\left(R_w\left\langle F_\beta - 1\right\rangle - \sin 2\theta_s\right)\beta_o + \left(R_w F_\zeta - \cos 2\theta_s\right)\zeta_o\right] \\
C_{\Delta\theta_s} &= \frac{R\bar{\omega}_\Delta^{2}}{\Delta}\left[\left(R_w C_\beta - \cos 2\theta_s\right)\beta_o + \left(R_w C_\zeta + \sin 2\theta_s\right)\zeta_o\right]
\end{aligned}
\right\} \quad (10)
$$

and where

$$
\left.
\begin{aligned}
\bar{\omega}_\Delta^{2} &= \bar{\omega}_\zeta^{2} - \bar{\omega}_\beta^{2} \\
\Delta &= 1 + R(1 - R)\frac{\bar{\omega}_\Delta^{4}}{\bar{\omega}_\zeta^{2}\bar{\omega}_\beta^{2}}\sin^2\theta_s \\
R_w &= (1 - R)\frac{\bar{\omega}_\Delta^{2}}{\bar{\omega}_\zeta^{2}\bar{\omega}_\beta^{2}}\sin 2\theta_s \\
\bar{\omega}_\beta^{2} &= K_\beta/I\Omega^2 \quad , \quad \bar{\omega}_\zeta^{2} = K_\zeta/I\Omega^2 \\
K_\beta &= \frac{K_{\beta_B}K_{\beta_H}}{K_{\beta_B} + K_{\beta_H}} \quad , \quad K_\zeta = \frac{K_{\zeta_B}K_{\zeta_H}}{K_{\zeta_B} + K_{\zeta_H}} \\
R_\beta &= K_\beta/K_{\beta_B} \quad , \quad R_\zeta = K_\zeta/K_{\zeta_B} \\
R &= \frac{\bar{\omega}_\zeta^{2}R_\beta - \bar{\omega}_\beta^{2}R_\zeta}{\bar{\omega}_\zeta^{2} - \bar{\omega}_\beta^{2}} \\
\phi_i &= \sqrt{\frac{\sigma c_{\ell_o}}{6}}
\end{aligned}
\right\} \quad (11)
$$

For linear aerodynamics (neglecting stall) the following substitutions are made.

$$\left.\begin{aligned} \phi_i &= \frac{a\sigma}{12}\left[\sqrt{1 + \frac{24\theta}{a\sigma}} - 1\right] \\ \alpha &= \theta - \phi_i \\ c_{\ell_o} &= a\alpha \\ c_{\ell_\alpha} &= a \\ c_{d_o} &= c_{d_p} \\ c_{d_\alpha} &= 0 \end{aligned}\right\} \quad (12)$$

The elastic parameters are defined by the blade root and hub spring systems shown in figure 20. The inclination of the blade spring system is given by θ_s which represents the inclination of the major (flapwise) principal flexural axis of the rotor blade. In the representation of figure 20 the [blade] pitch angle is given by θ which is the aerodynamic pitch angle. The blade and the blade spring system are fixed together and rotate about the pitch bearing. When $\theta = 0$, the blade spring system inclination is θ_{s_o} since $\theta_s = \theta_{s_o} + \theta$. The hub spring system axes are always aligned orthogonal to the rotor shaft axis/plane of rotation. The angles θ_s and θ are considered to be the structural and aerodynamic pitch angles of the blade. respectively. In this report, only configurations having $R_\beta = R_\zeta = R = 1.0$ are considered. For this case, $\Delta = 1.0$ and $R_w = 0$. Perturbations in the aerodynamic and structural pitch angles of the blade are both equal to $\Delta\theta$ which is given by the pitch-flap and pitch-lag coupling relation

$$\Delta\theta = \theta_\beta \Delta\beta + \theta_\zeta \Delta\zeta \quad (13)$$

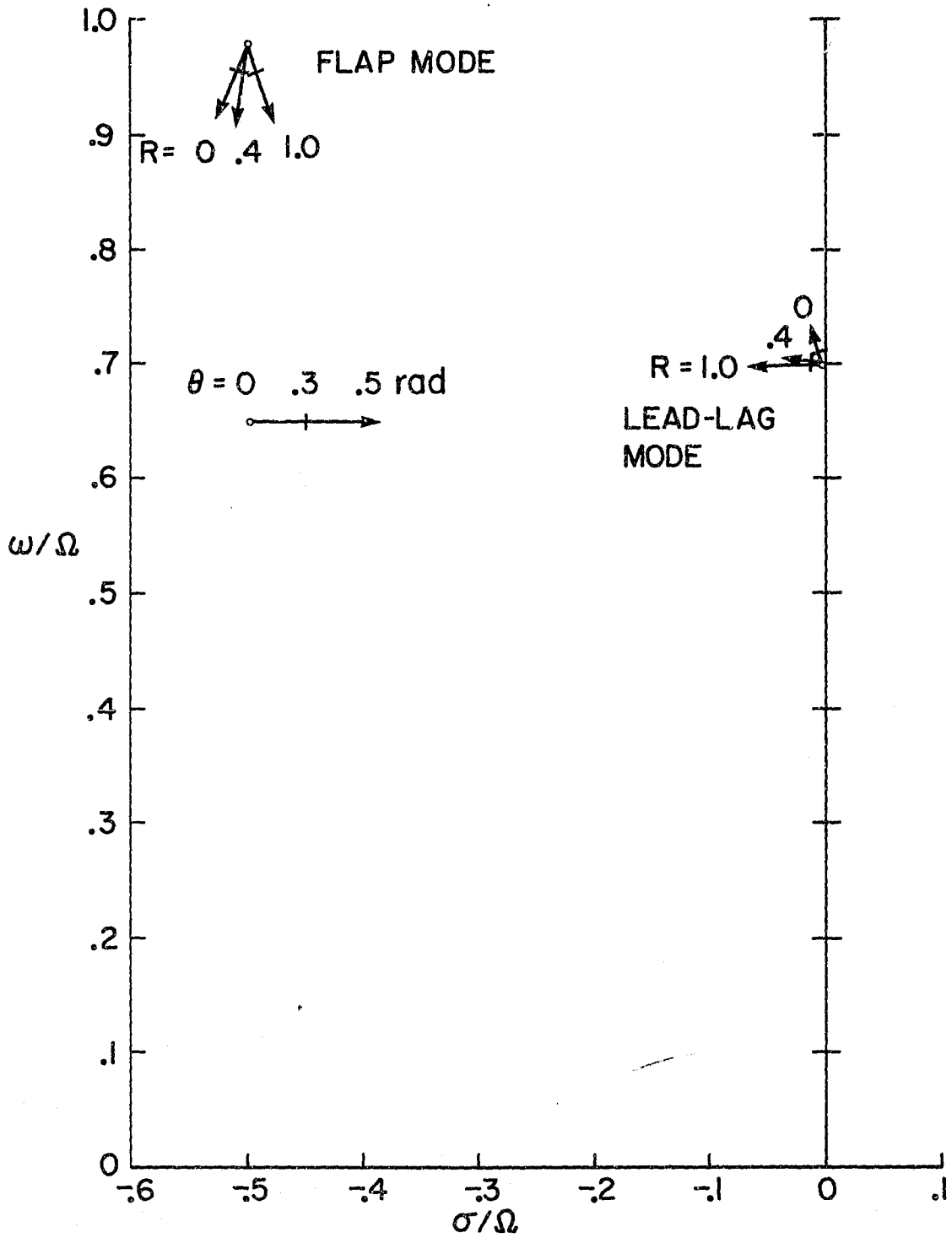

Figure 1. Effect of flap-lag elastic coupling on basic flap-lag locus of roots, $p = 1.1$, $\bar{\omega}_\zeta = 0.7$, $\gamma = 8.0$, $c_{d_p} = .01$, $\sigma = .05$, $\theta_{s_o} = \theta_\zeta = \theta_\beta = 0$.

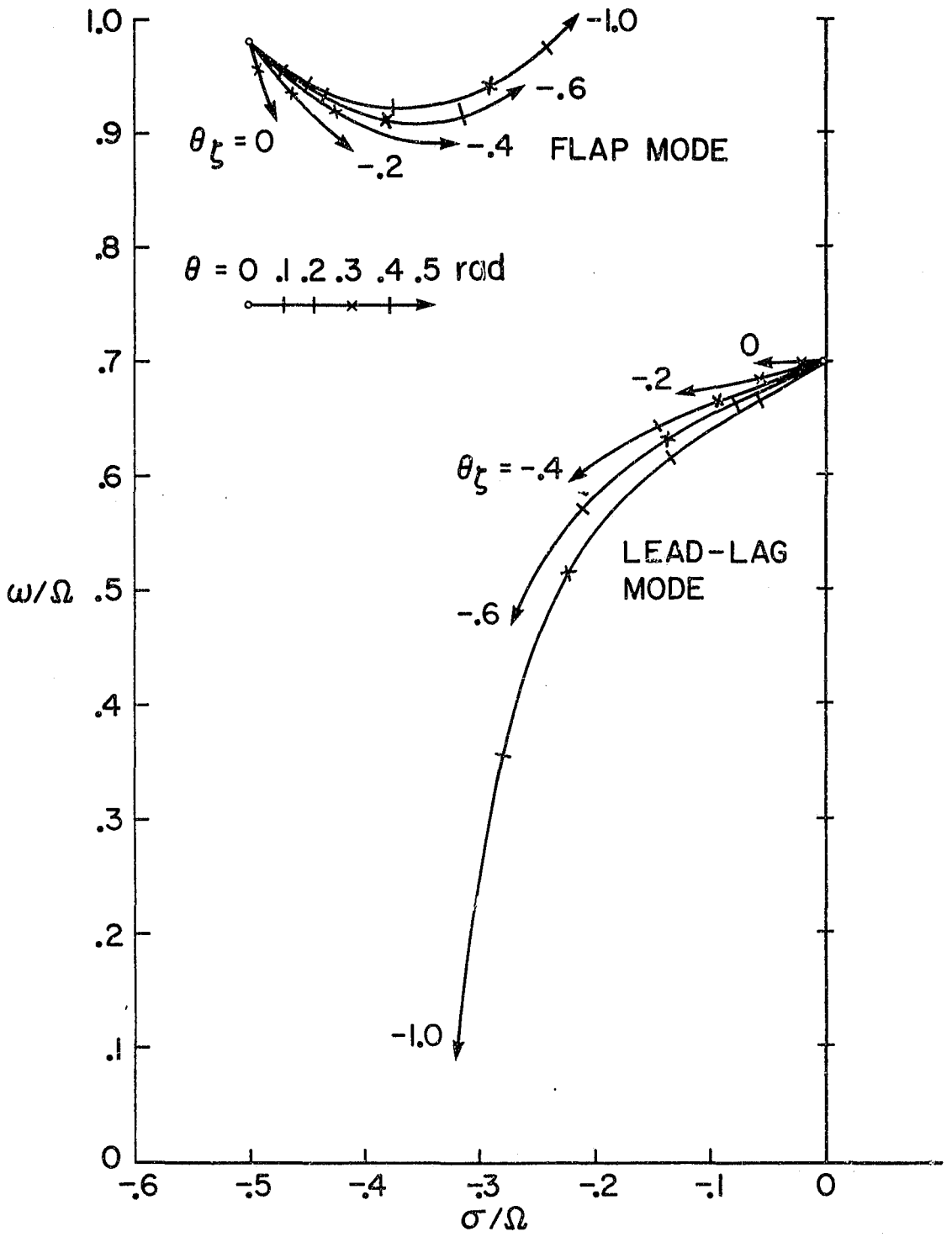

Figure 2. Effect of pitch-lag coupling on basic flap-lag locus of roots, p = 1.1, $\bar{\omega}_\zeta$ = 0.7, γ = 8.0, c_{d_p} = .01, σ = .05, $\theta_{s_o} = \theta_\beta$ = 0, R = 1.0.

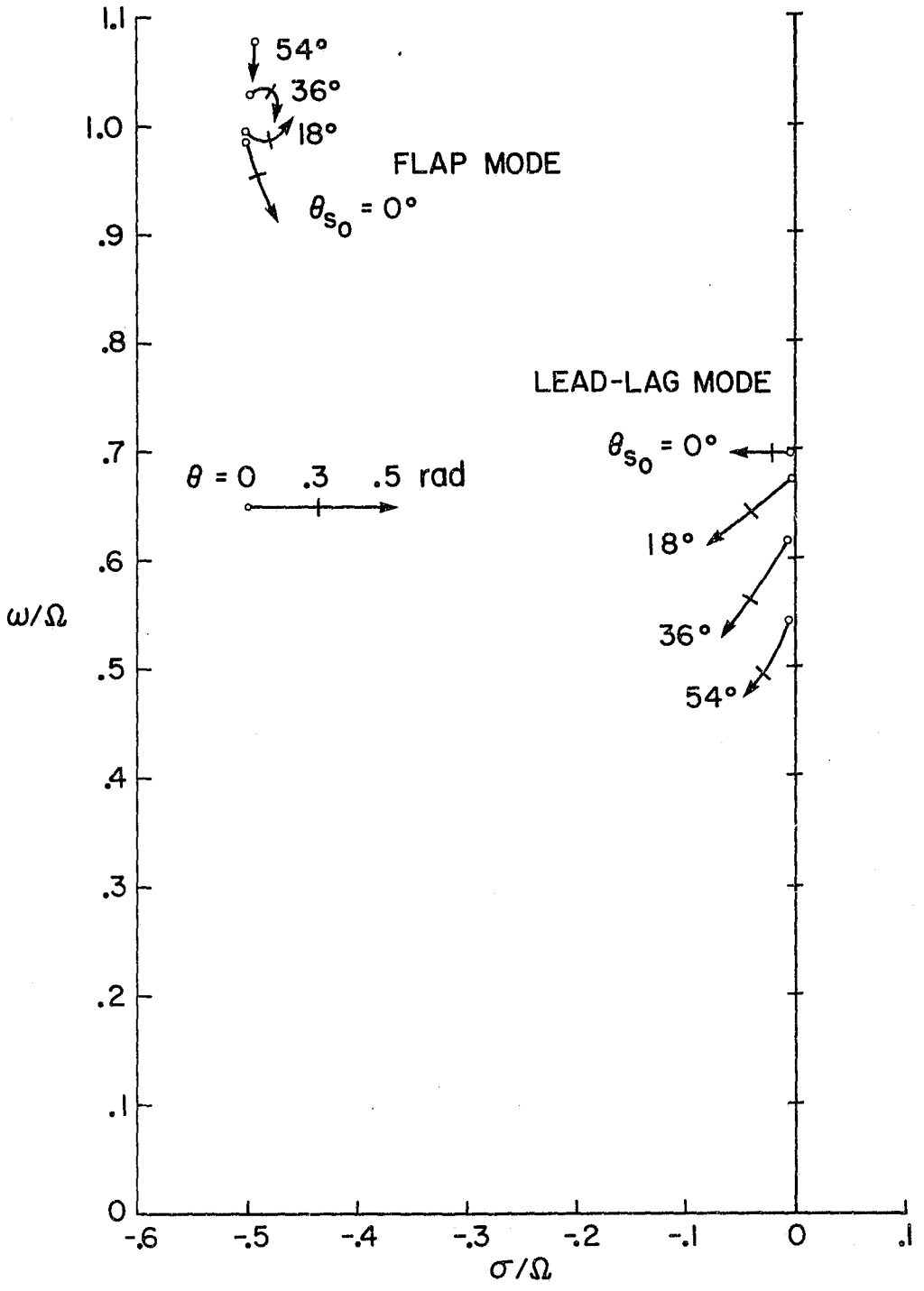

Figure 3. Effect of inclining principal flexural axes of blade with respect to blade chord line on the flap-lag locus of roots, p = 1.1, $\bar{\omega}_\zeta$ = 0.7, γ = 8, c_{d_p} = .01, σ = .05, $\theta_\zeta = \theta_\beta$ = 0, R = 1.0.

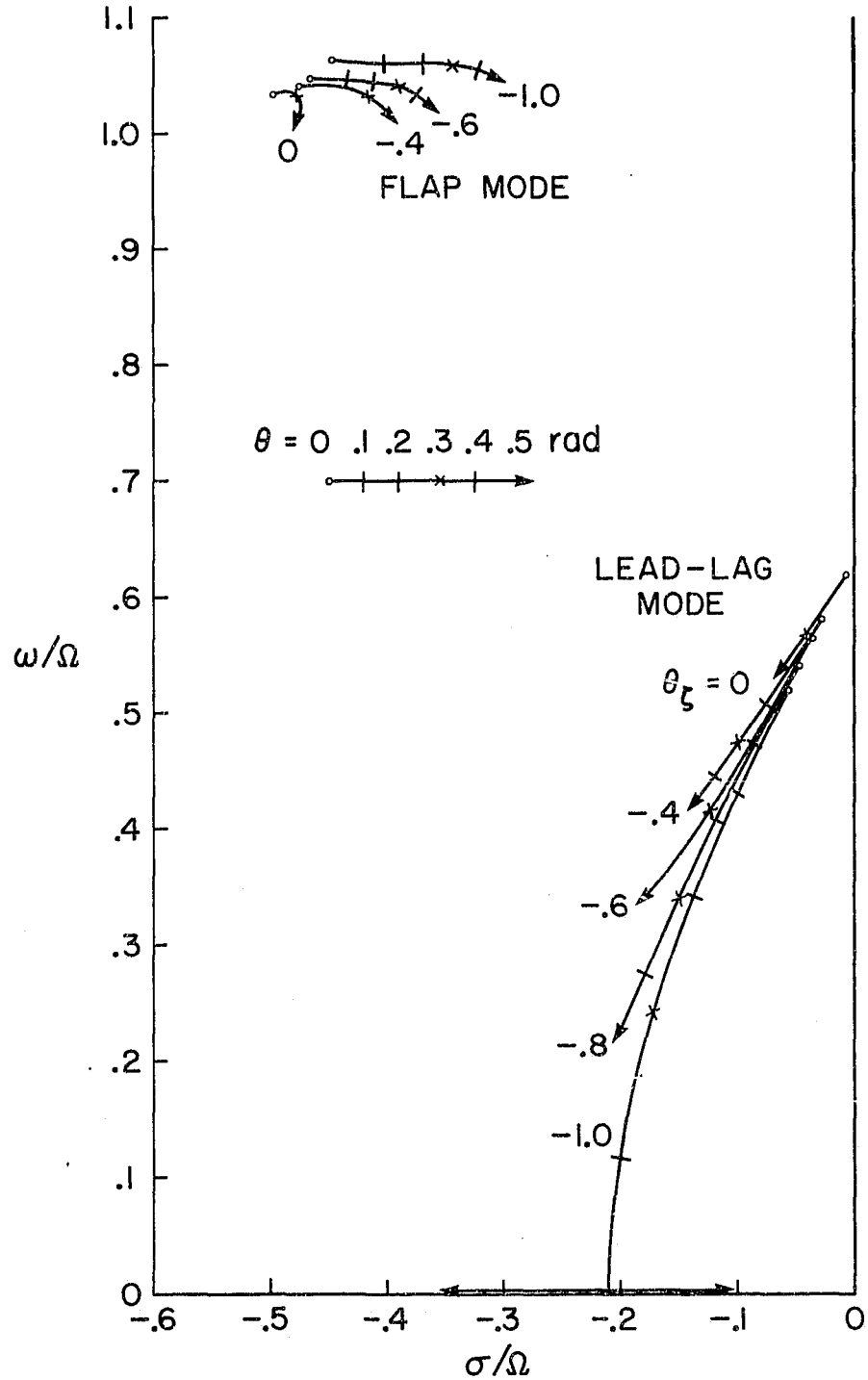

Figure 4. Effect of inclined principal flexural axes and pitch-lag coupling on flap-lag locus of roots, p = 1.1, $\bar{\omega}_\zeta$ = 0.7, γ = 8, c_{d_p} = .01, σ = .05, θ_β = 0, θ_{s_o} = 36°, R = 1.0.

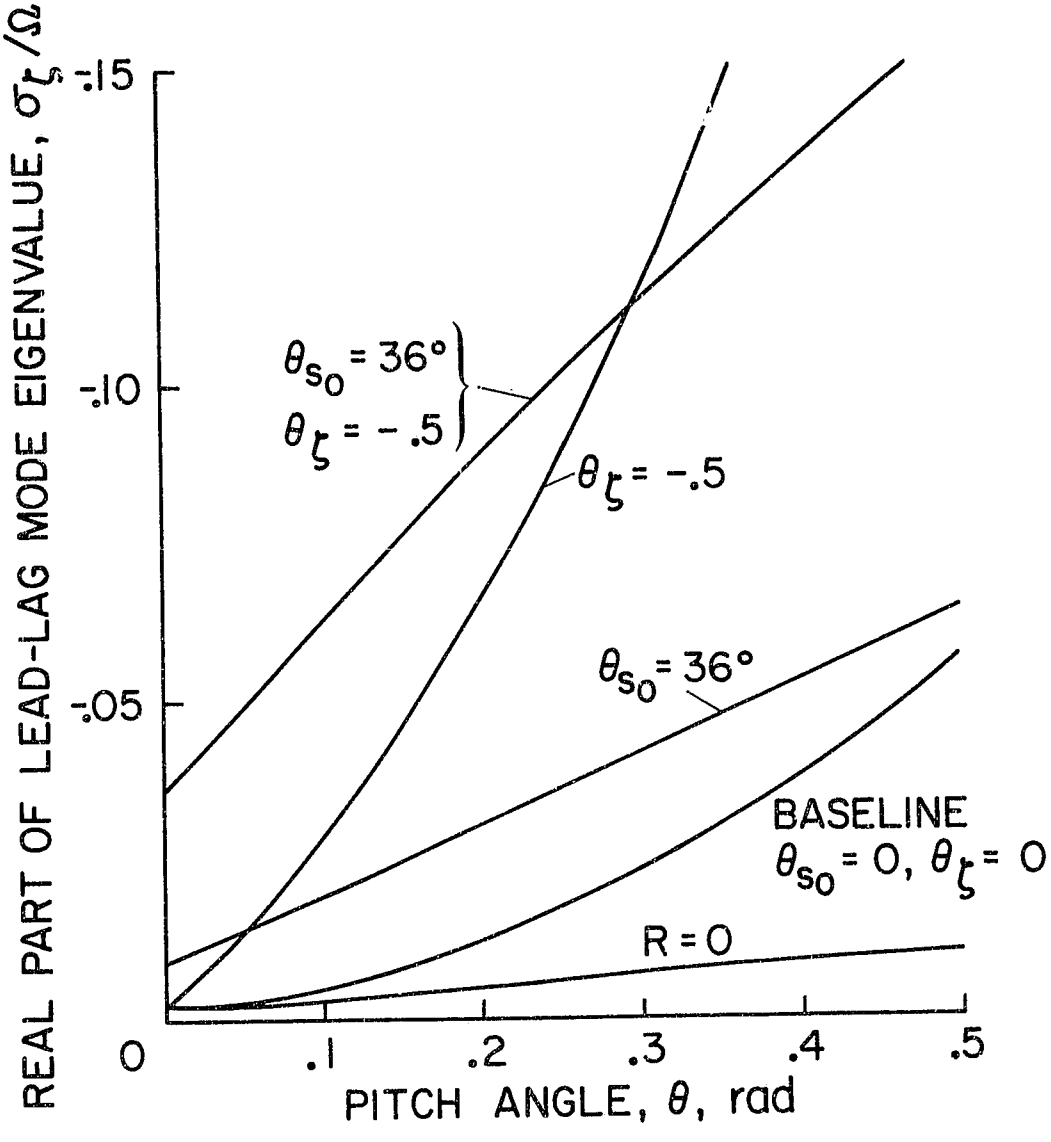

Figure 5. Summary comparison of effects of coupling on lead-lag damping versus blade pitch angle, p = 1.1, $\bar{\omega}_\zeta$ = 0.7, γ = 8, c_{d_p} = .01, σ = .05, θ_β = 0, R = 1.0.

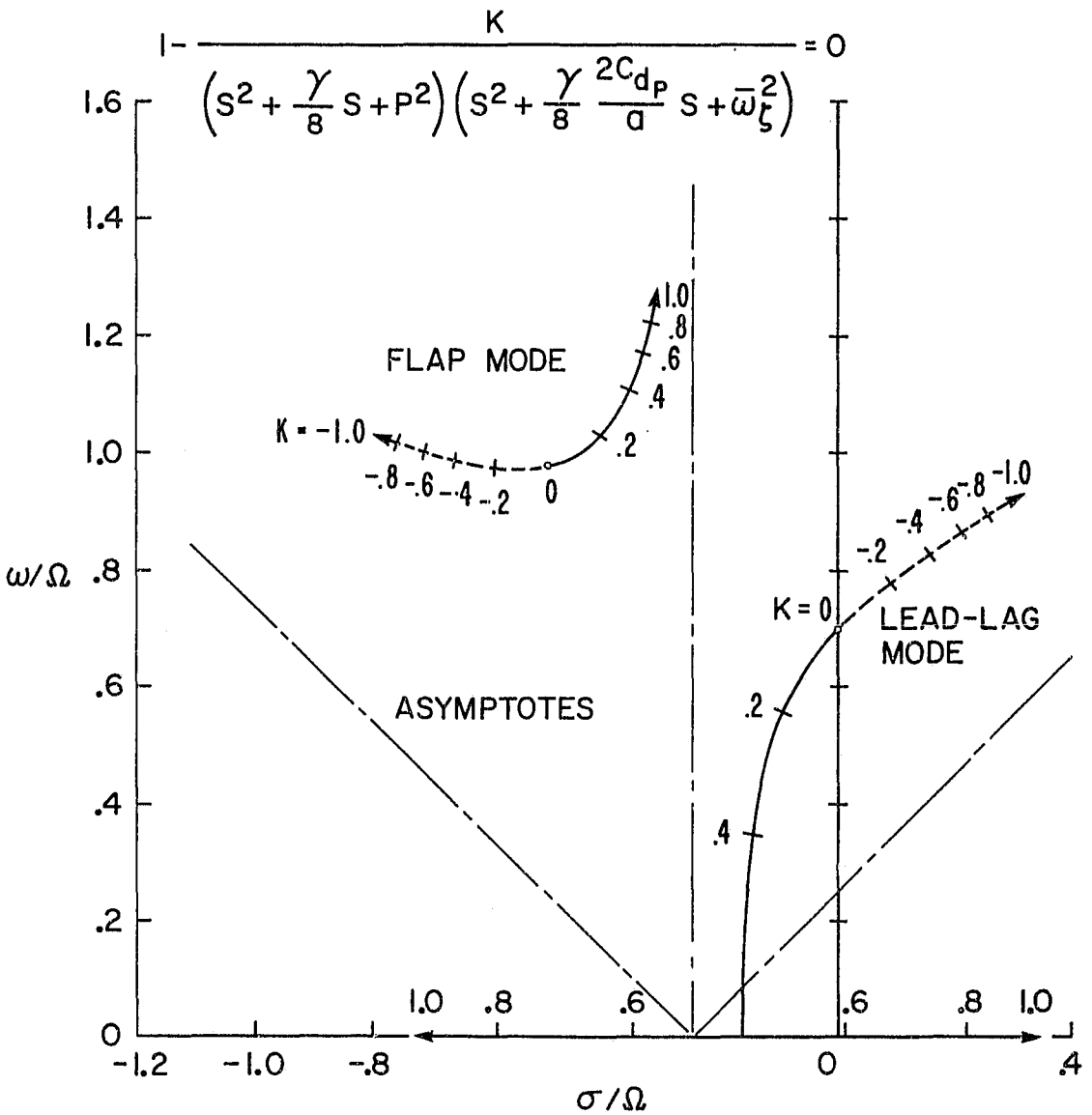

Figure 6. Flap-lag root locus with coupling parameter K varying, p = 1.1, $\bar{\omega}_\zeta = 0.7$, $\gamma = 8$, $2c_{d_p}/a = .01/\pi$.

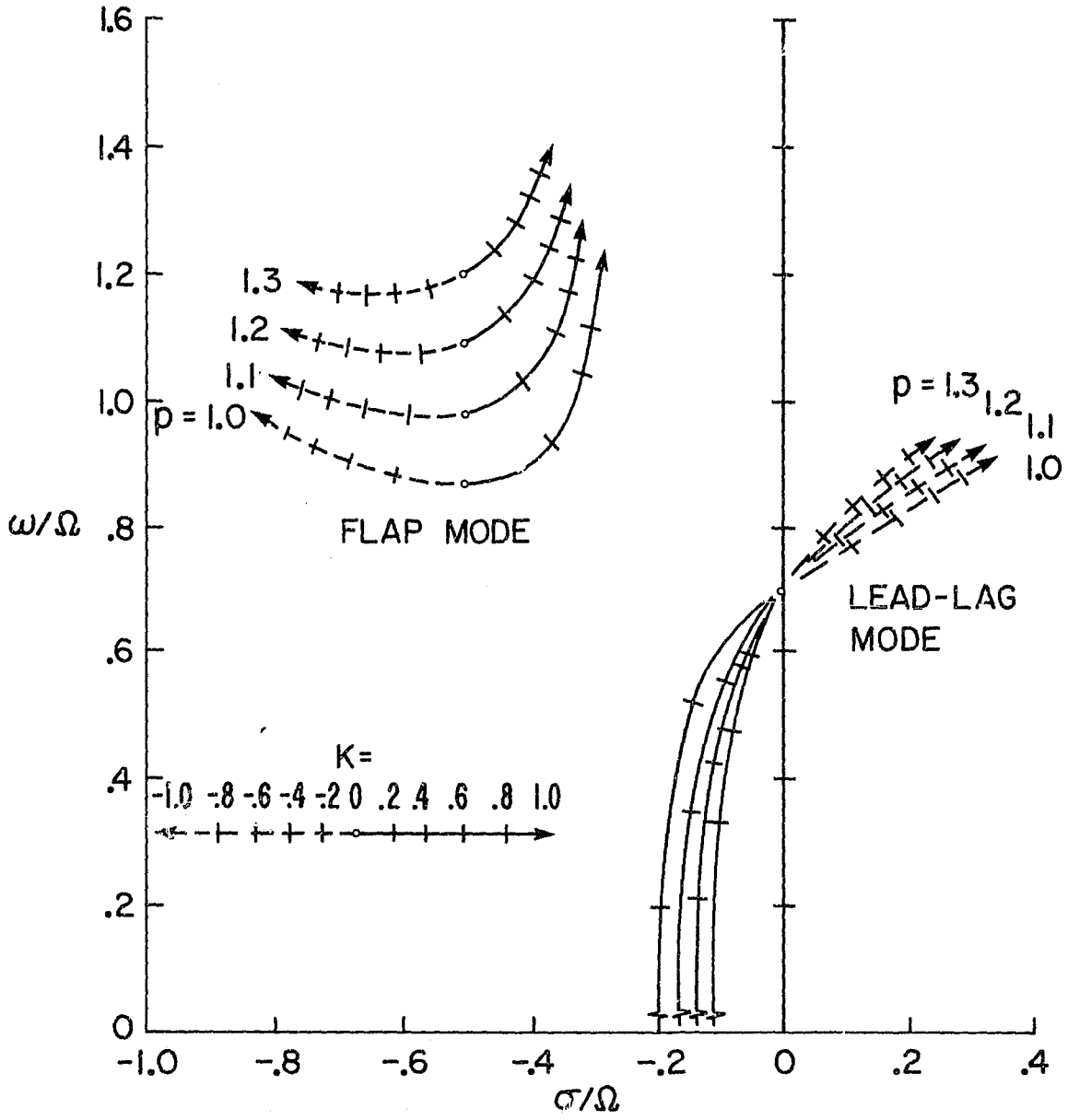

Figure 7. Effect of uncoupled flap frequency on flap-lag root locus with coupling parameter K varying, $\bar{\omega}_\zeta = 0.7$, $\gamma = 8$, $2c_{d_p}/a = .01/\pi$.

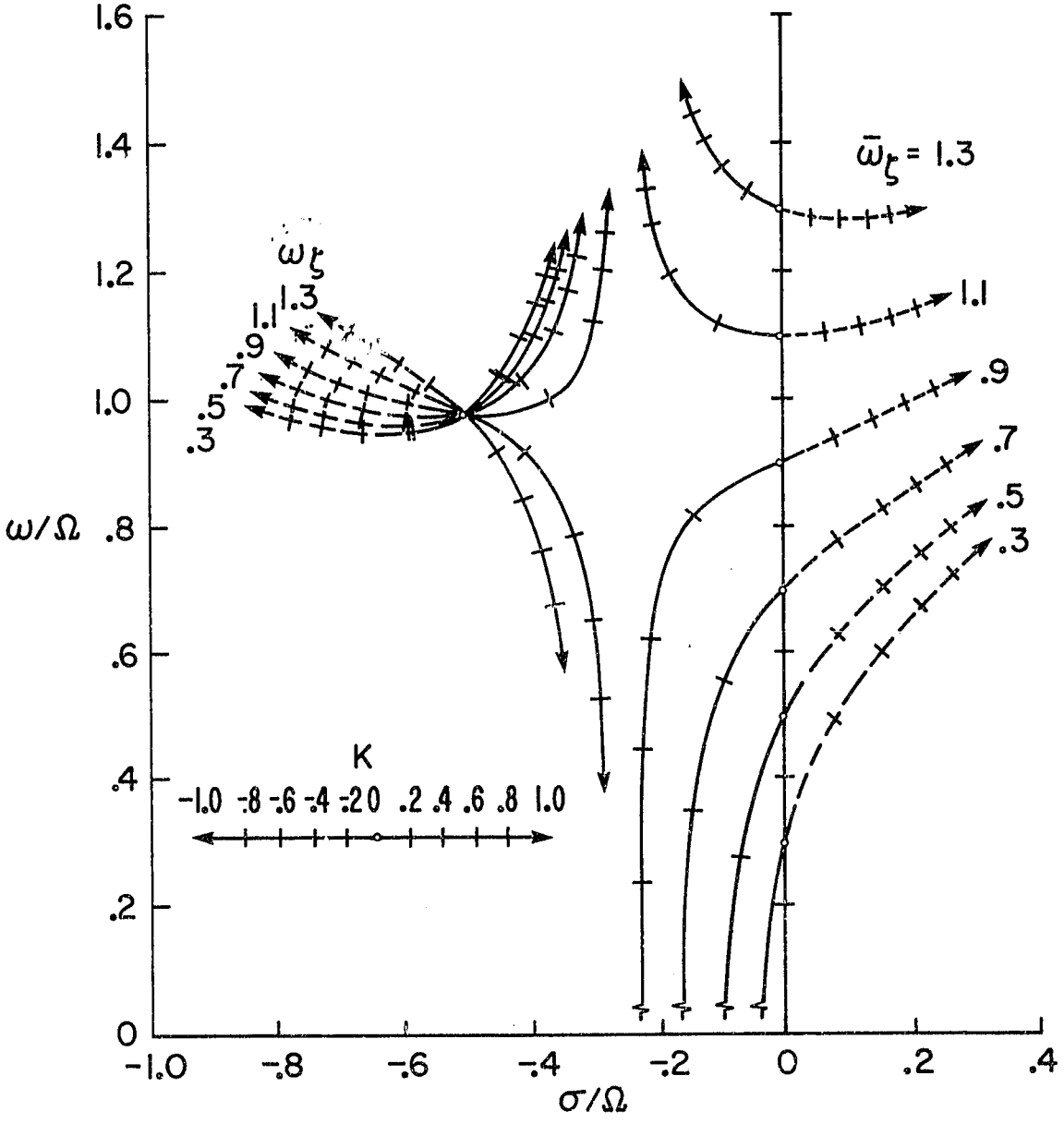

Figure 8. Effect of uncoupled lead-lag frequency on flap-lag root locus with coupling parameter K varying, p = 1.1, γ = 8, $2c_{d_p}/a = .01/\pi$.

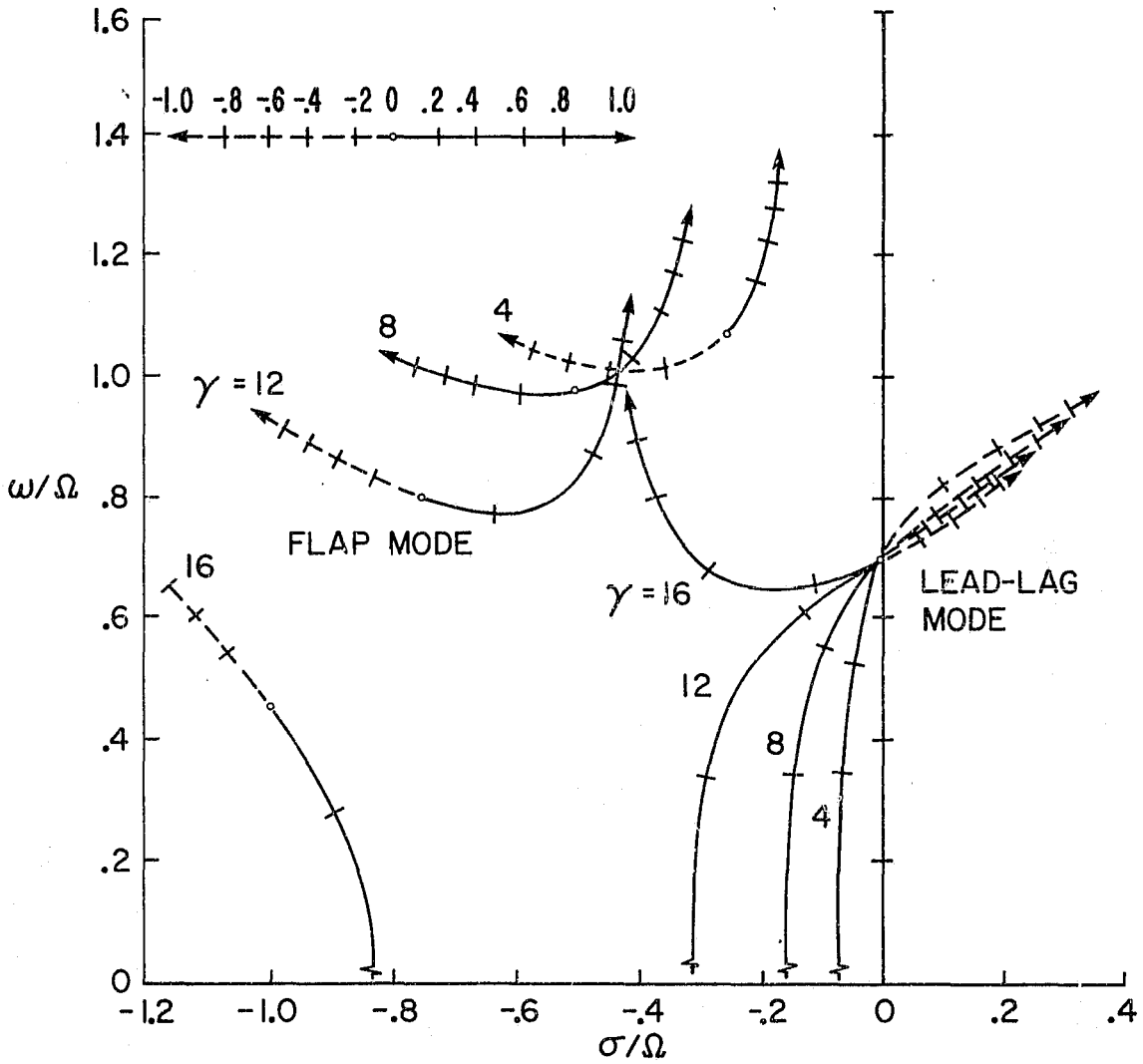

Figure 9. Effect of Lock number on flap-lag root locus with coupling parameter K varying, p = 1.1, $\bar{\omega}_\zeta$ = 0.7, $2c_{d_p}/a = .01/\pi$.

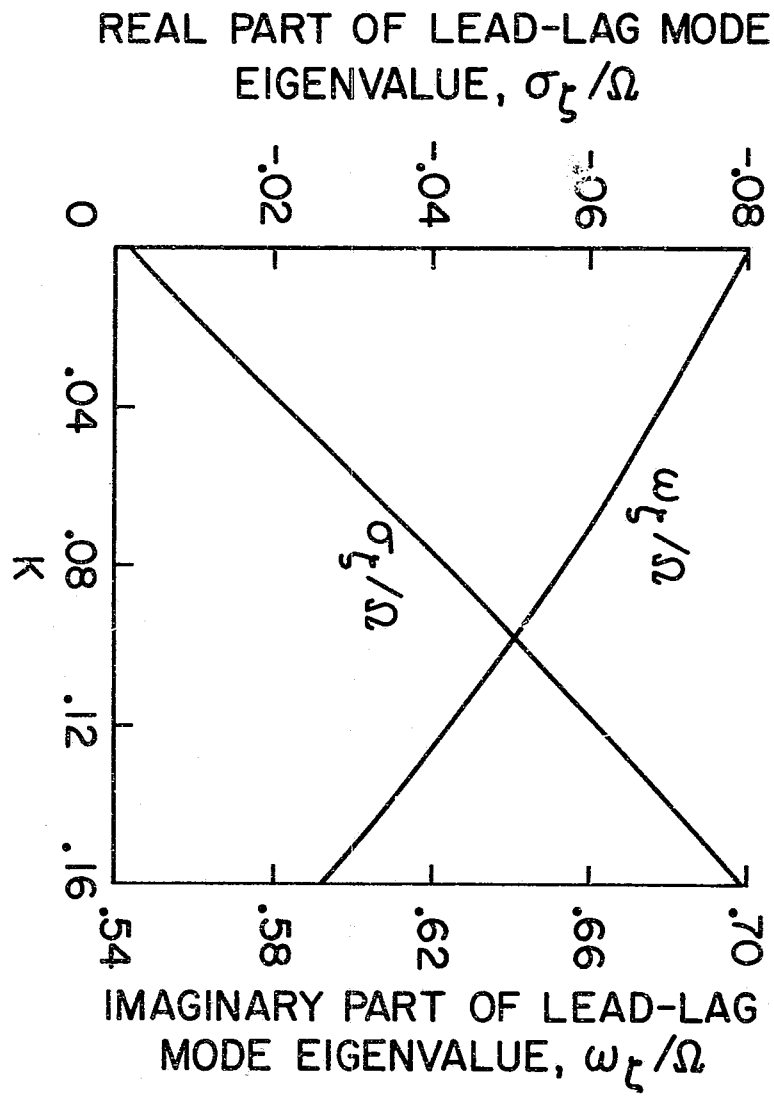

Figure 10. Lead-lag mode frequency and damping versus the coupling parameter K, p = 1.1, $\bar{\omega}_\zeta$ = 0.7, γ = 8, $2c_{d_p}/a = .01/\pi$.

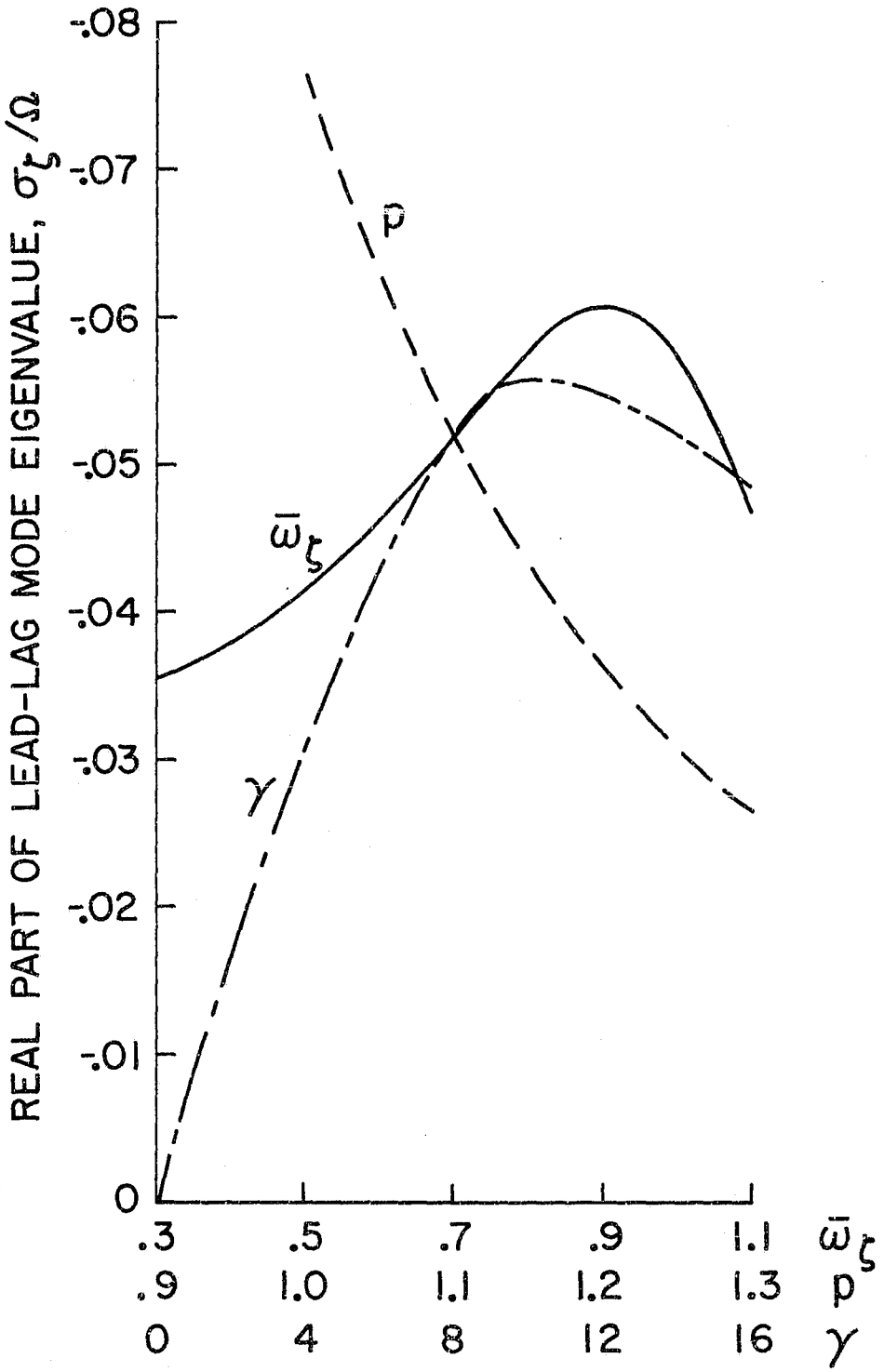

Figure 11. Sensitivity of lead-lag damping to basic system parameters, baseline configuration, $p = 1.1$, $\bar{\omega}_\zeta = 0.7$, $\gamma = 8$, $2c_{d_p}/a = .01/\pi$, $K = 0.1$.

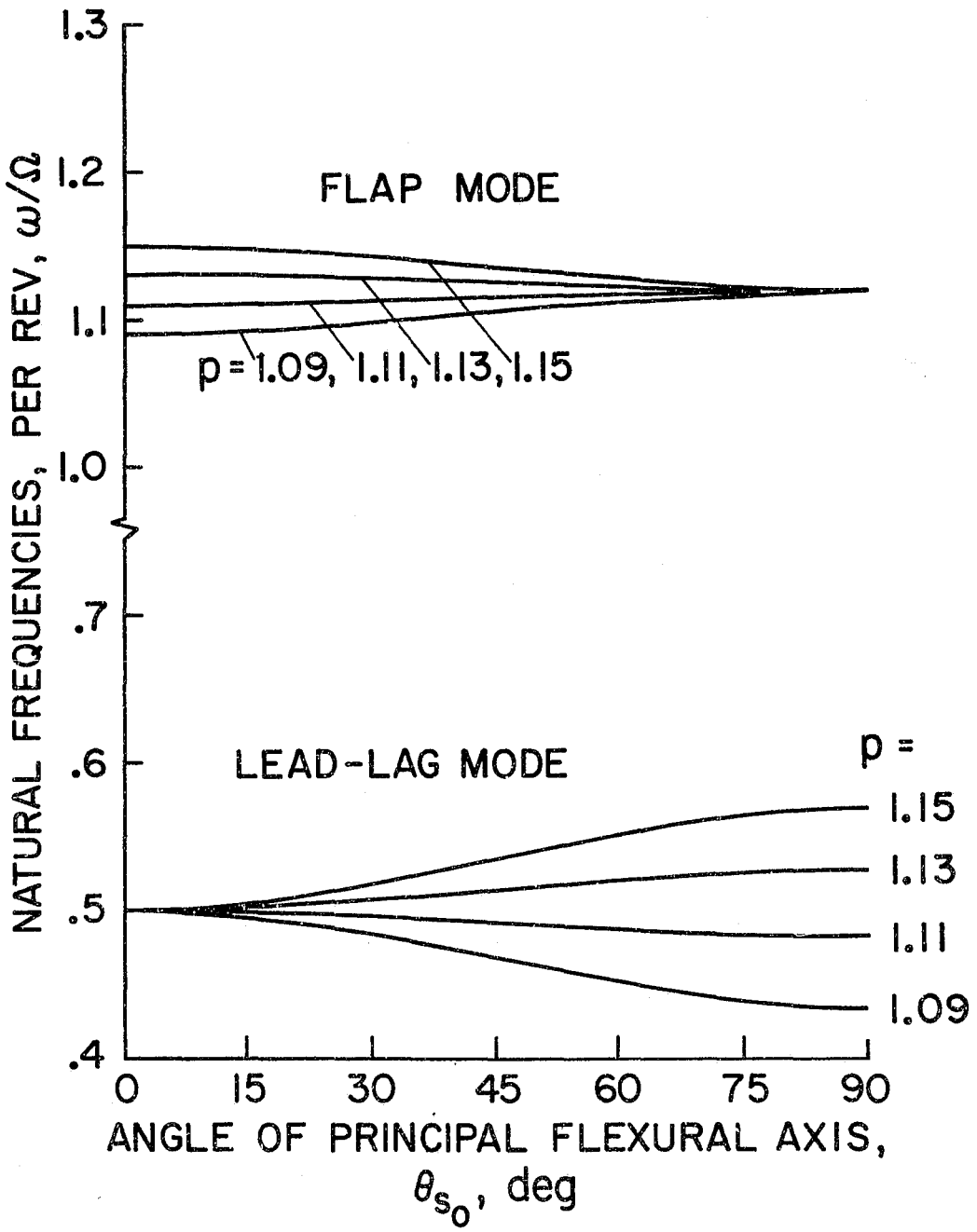

(a) Uncoupled lead-lag frequency $\bar{\omega}_\zeta = 0.5$.

Figure 12. Flap and lead-lag natural frequencies as a function of inclination of the principal flexural axes.

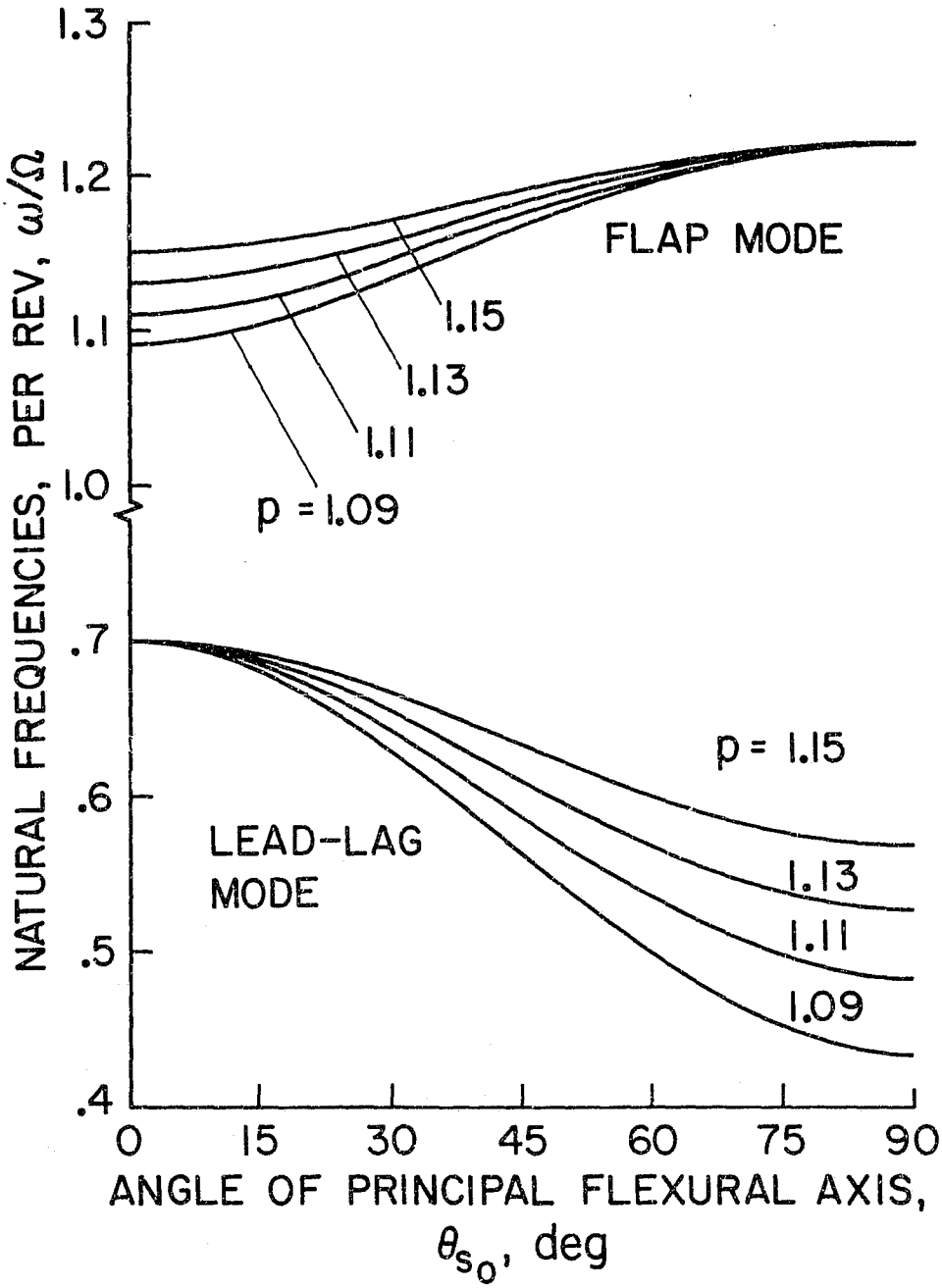

(b) Uncoupled lead-lag frequency $\bar{\omega}_\zeta = 0.7$.

Figure 12. Concluded.

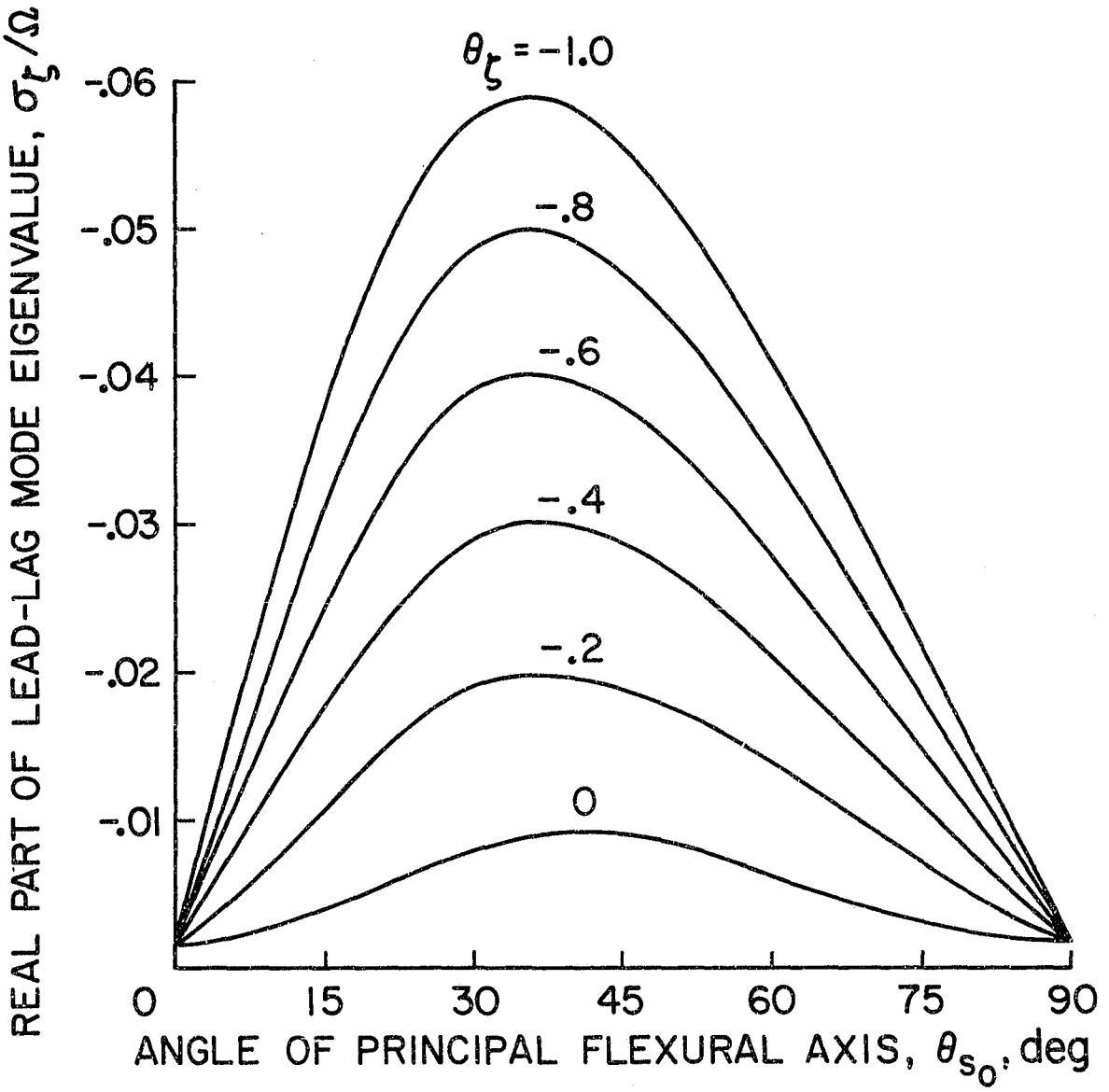

(a) $\theta_\beta = 0.$

Figure 13. Effect of inclination of principal flexural axes on lead-lag mode damping at zero pitch angle ($\theta = 0°$), $p = 1.1$, $\bar{\omega}_\zeta = 0.7$, $\gamma = 8$, $2c_{d_p}/a = .01/\pi$, $R = 1.0$.

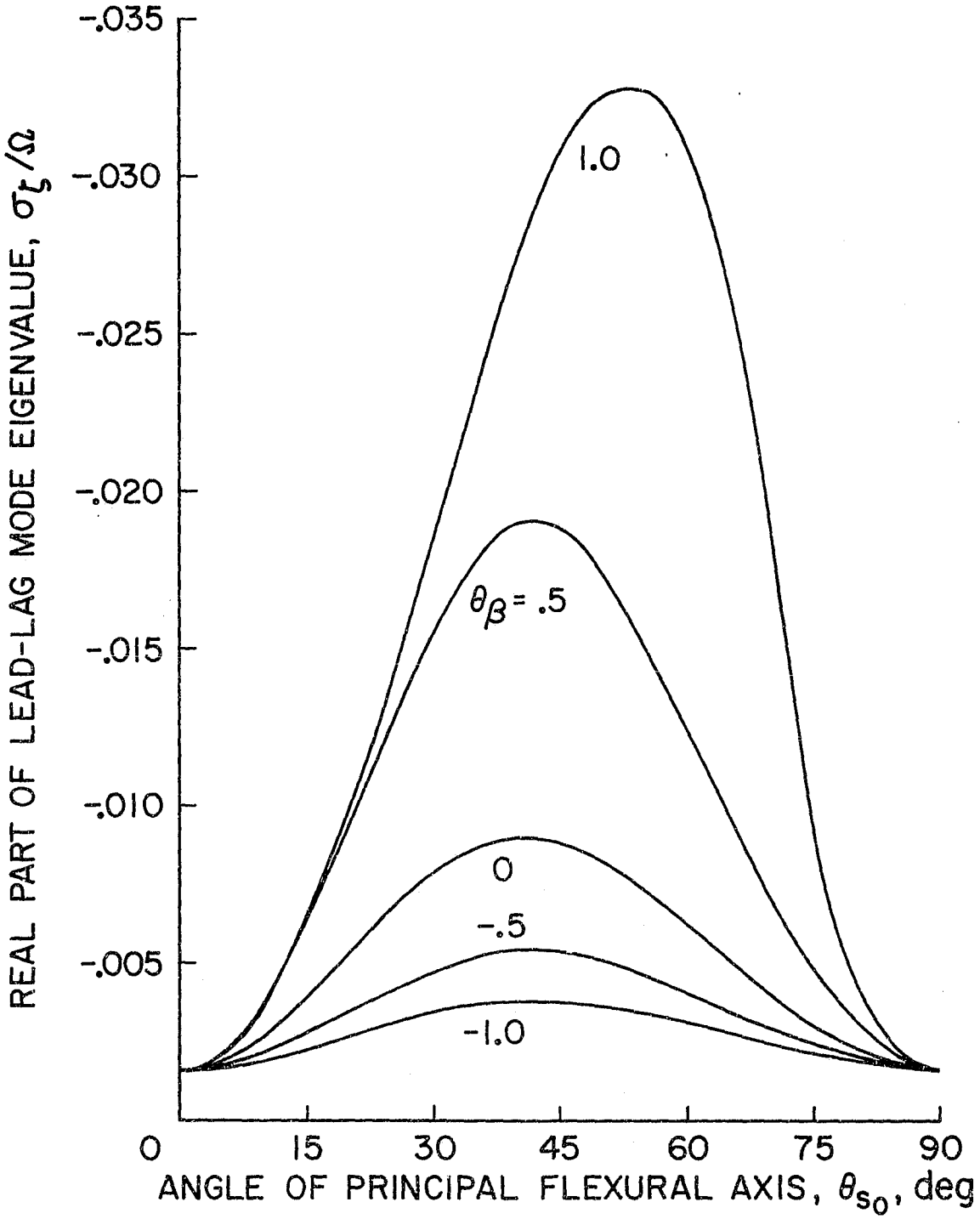

(b) $\theta_\zeta = 0.$

Figure 13. Concluded.

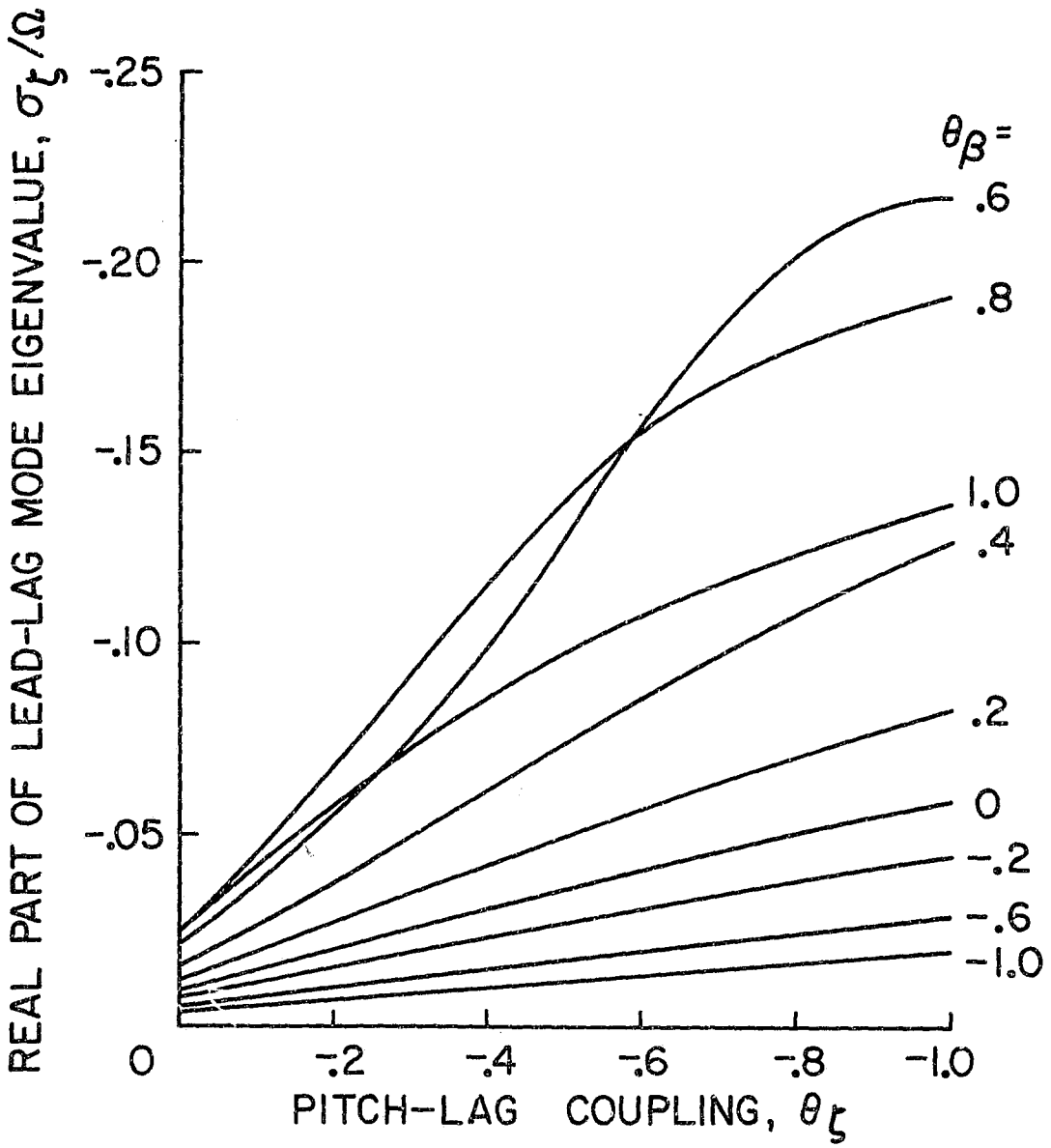

(a) σ_ζ/Ω versus θ_ζ, θ_β constant.

Figure 14. Effect of pitch-lag and pitch-flap coupling on lead-lag mode damping at zero pitch angle ($\theta = 0°$), $p = 1.1$, $\bar{\omega}_\zeta = 0.7$, $\gamma = 8$, $2c_{d_p}/a = .01/\pi$, $\theta_{s_o} = 36°$, $R = 1.0$.

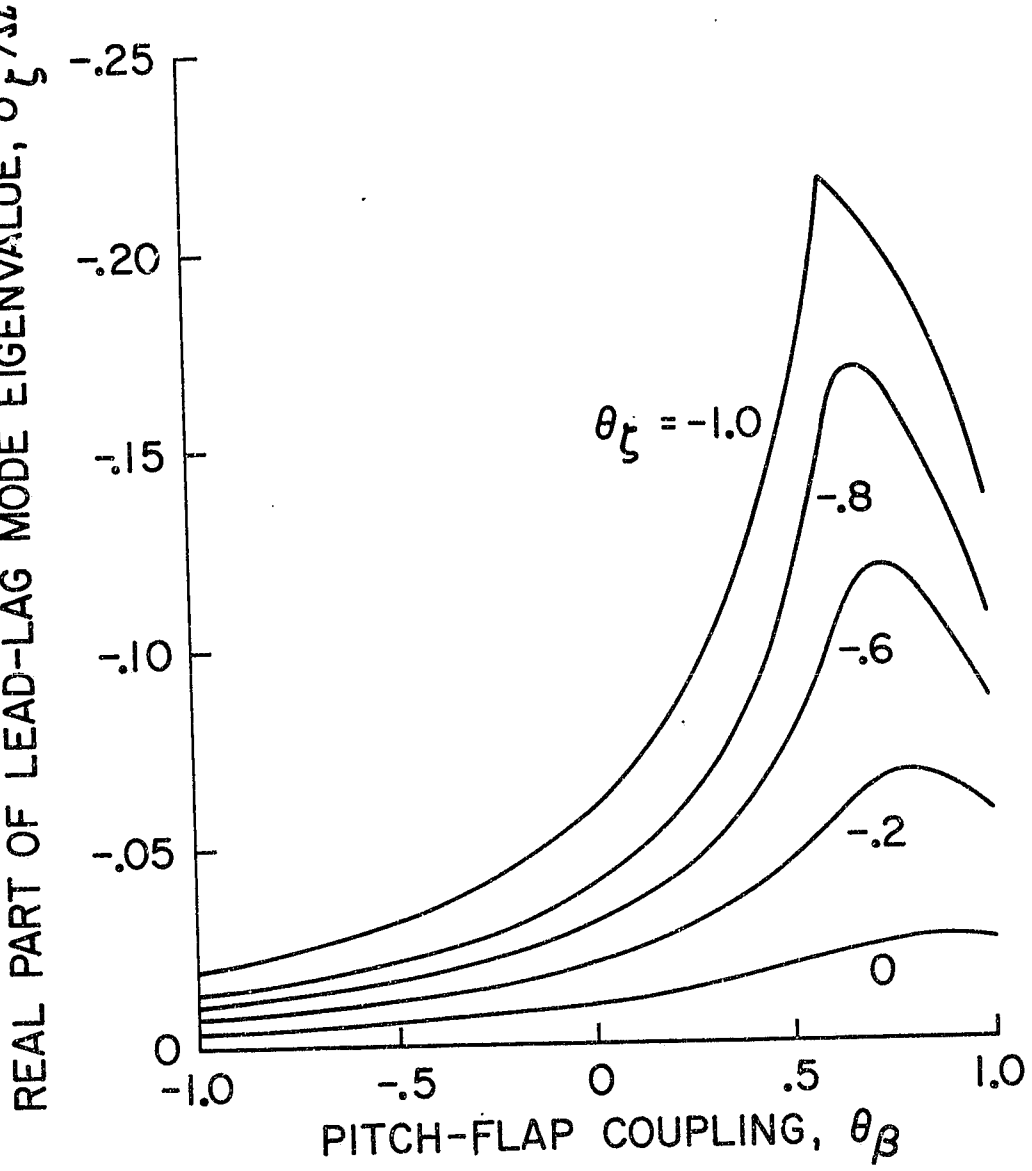

(b) σ_ζ/Ω versus θ_β, θ_ζ constant.

Figure 14. Concluded.

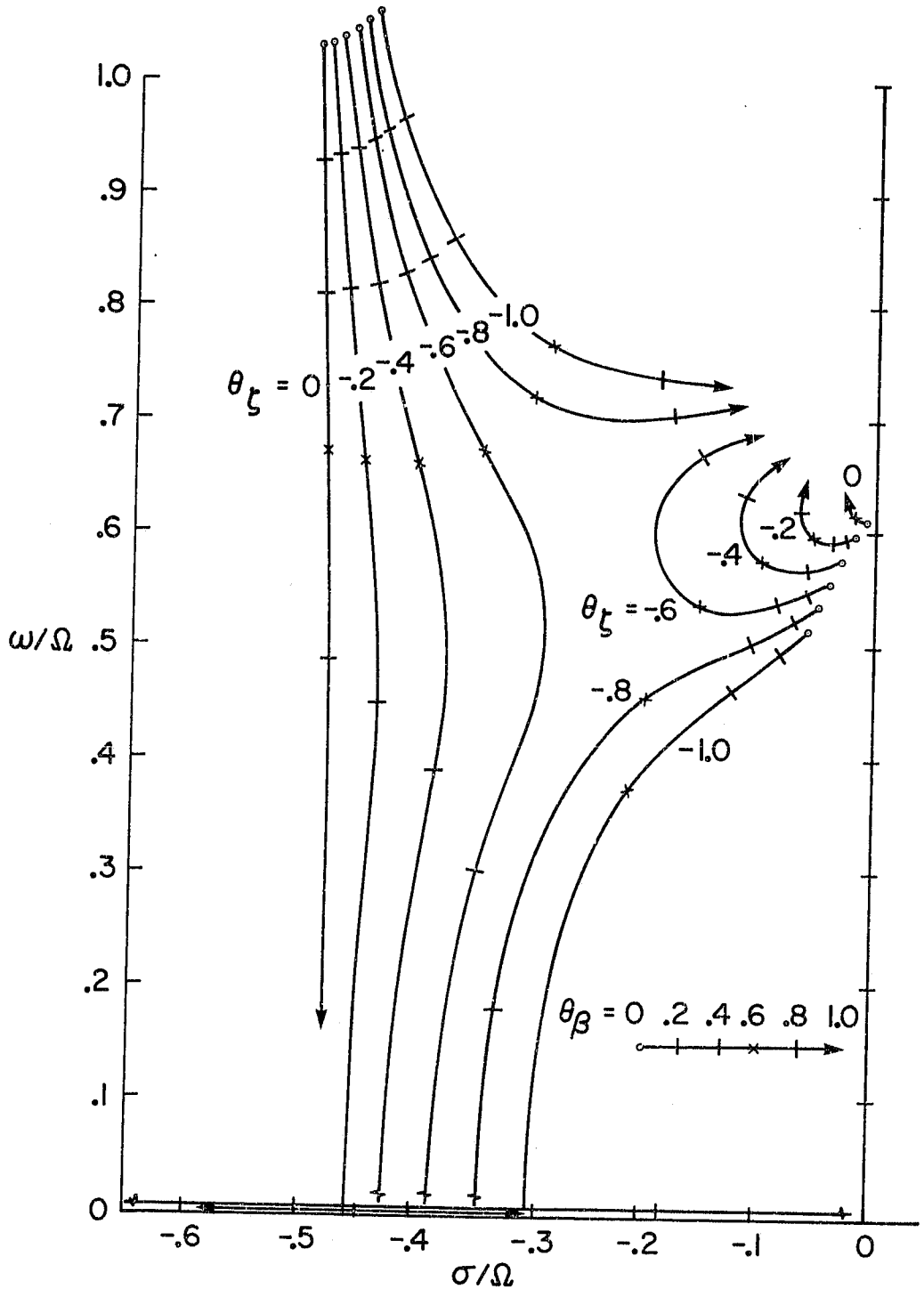

Figure 15. Effect of pitch-lag and pitch-flap coupling on flap-lag locus of roots, θ_β varying; p = 1.1, $\bar{\omega}_\zeta$ = 0.7, γ = 8, $2c_{d_p}/a = .01/\pi$, $\theta_{s_o} = 36°$, R = 1.0.

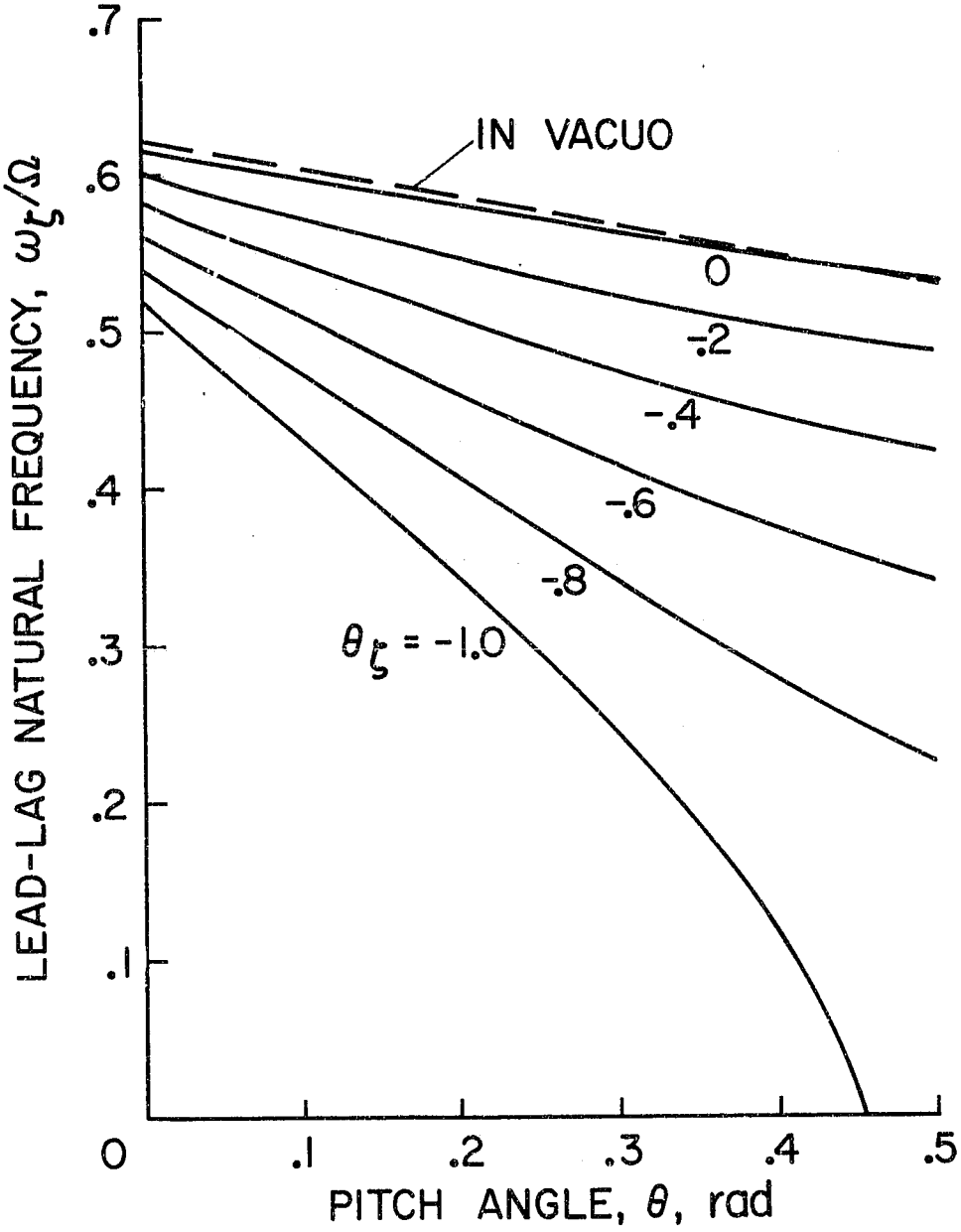

Figure 16. Effect of pitch-lag coupling on lead-lag frequency versus blade pitch angle, p = 1.1, $\bar{\omega}_\zeta$ = 0.7, γ = 8, $2c_{d_p}/a = .01/\pi$, θ_{s_o} = 36°, R = 1.0.

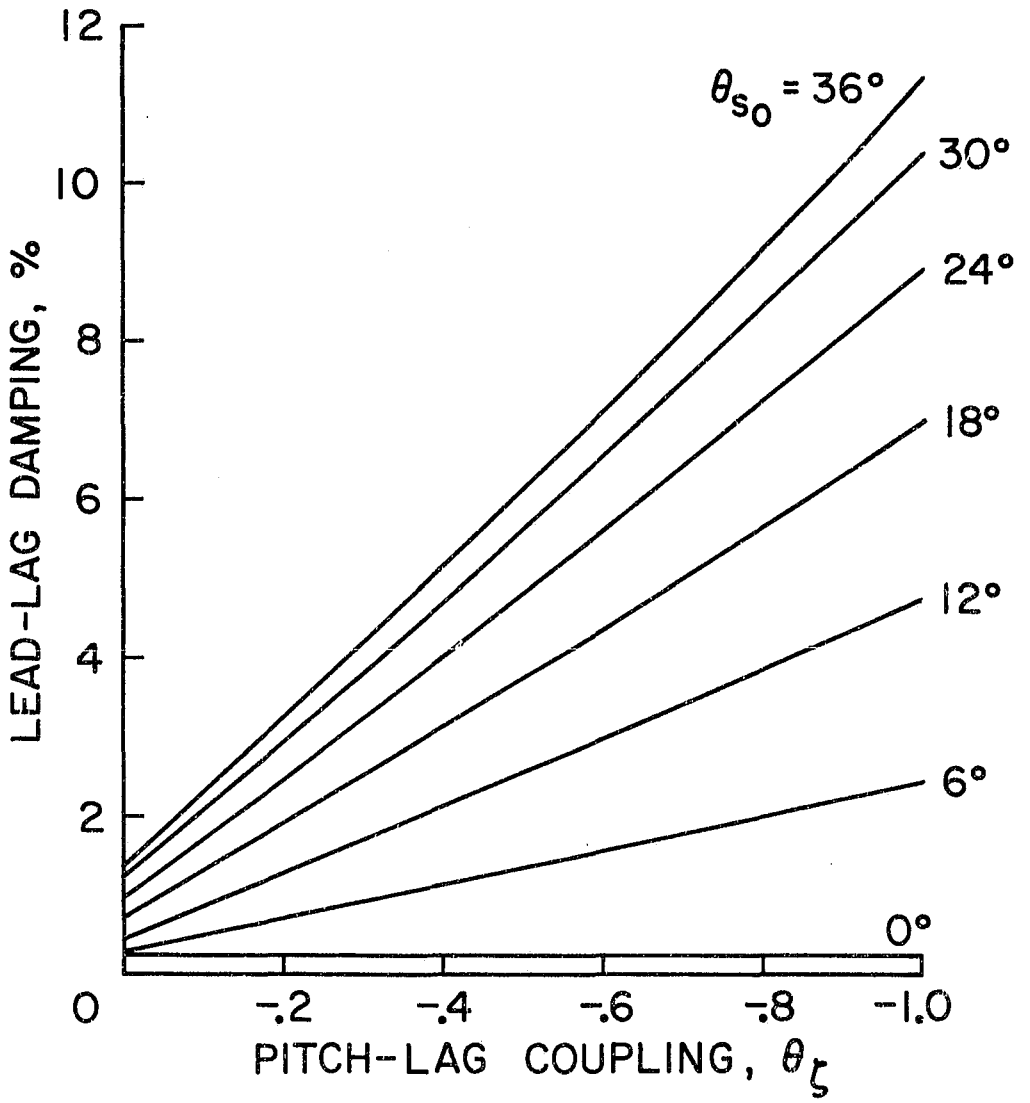

(a) p = 1.1, $\bar{\omega}_\zeta$ = 0.7, γ = 8.

Figure 17. Percent critical lead-lag damping as a function of pitch-lag coupling and principal flexural axis inclination, $2c_{d_p}/a = .01/\pi$, R = 1.0.

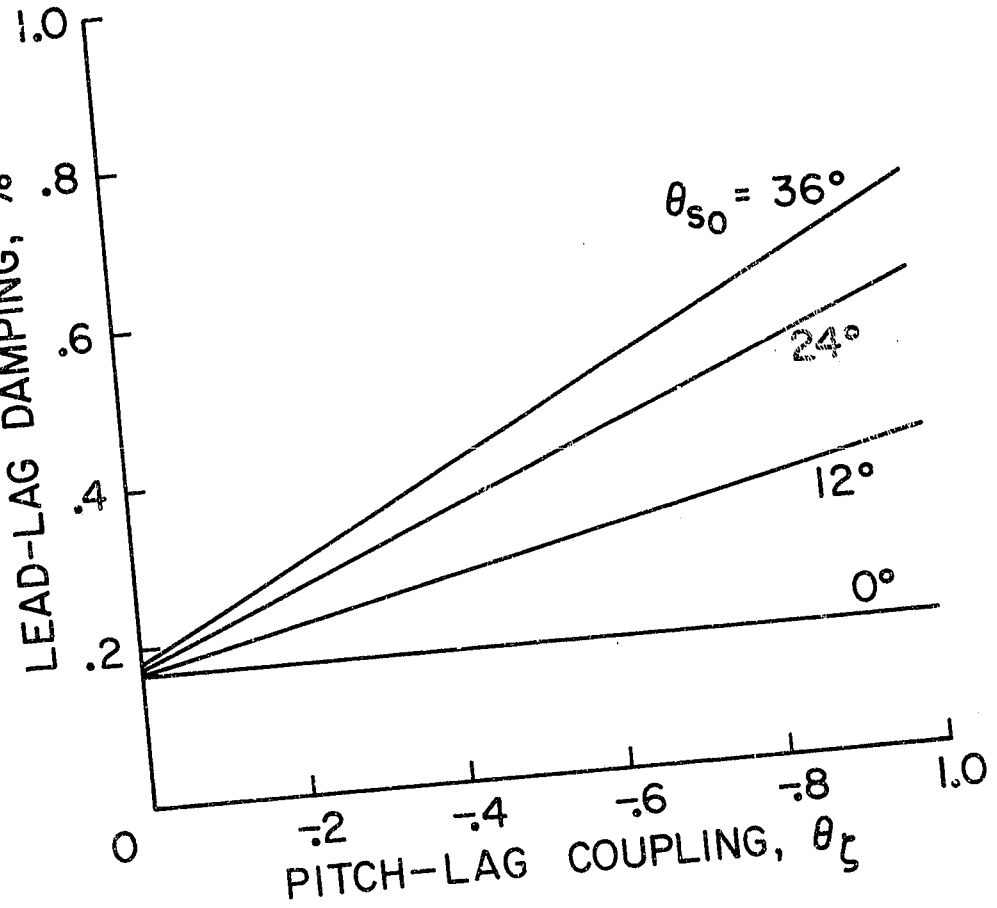

(b) $p = 1.15$, $\bar{\omega}_\zeta = 0.5$, $\gamma = 5$.

Figure 17. Concluded.

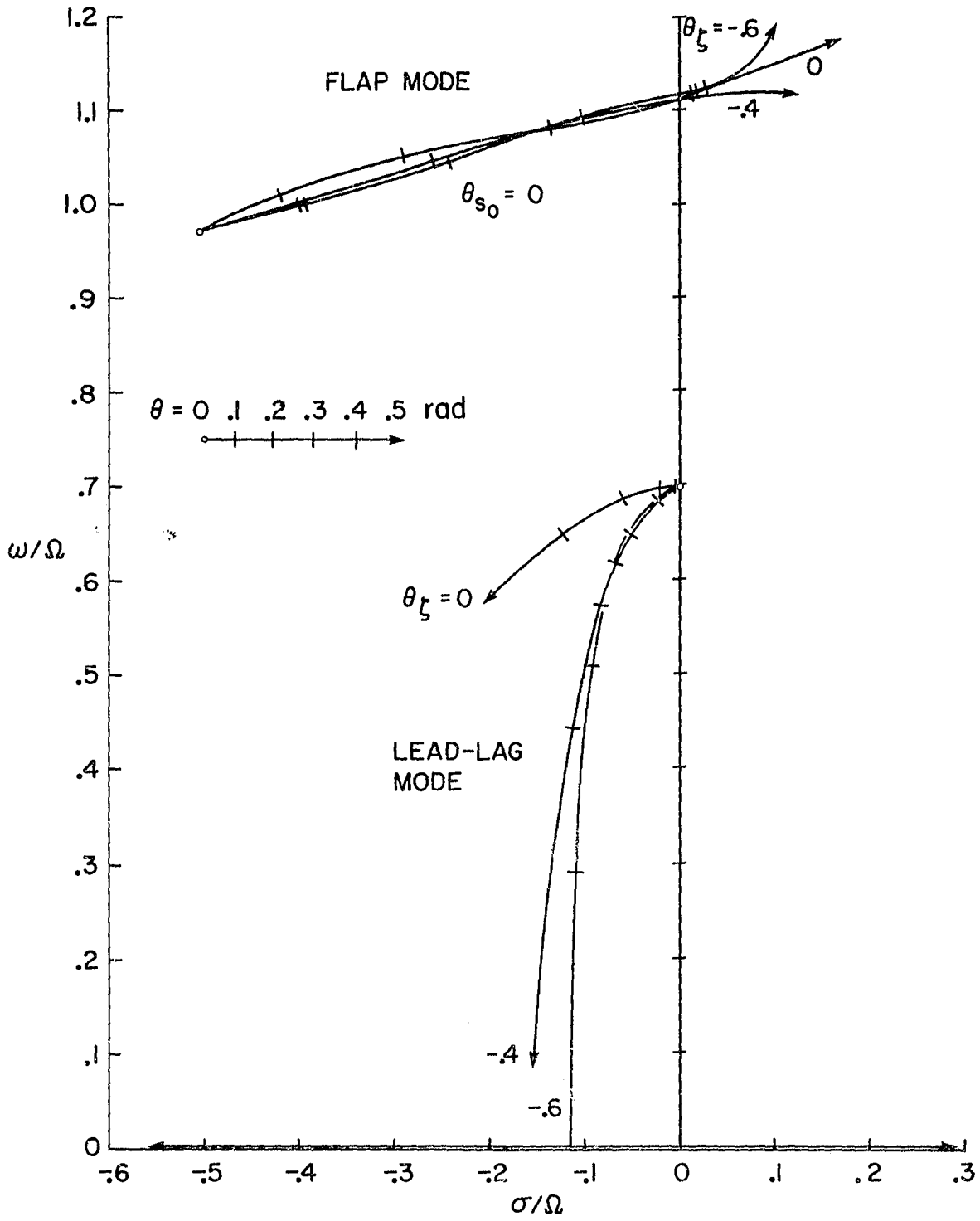

Figure 18. Effect of stall on flap-lag locus of roots with pitch-lag coupling, $p = 1.1$, $\bar{\omega}_{\zeta} = 0.7$, $\gamma = 8$, $\theta_{s_o} = 0$, $R = 1.0$.

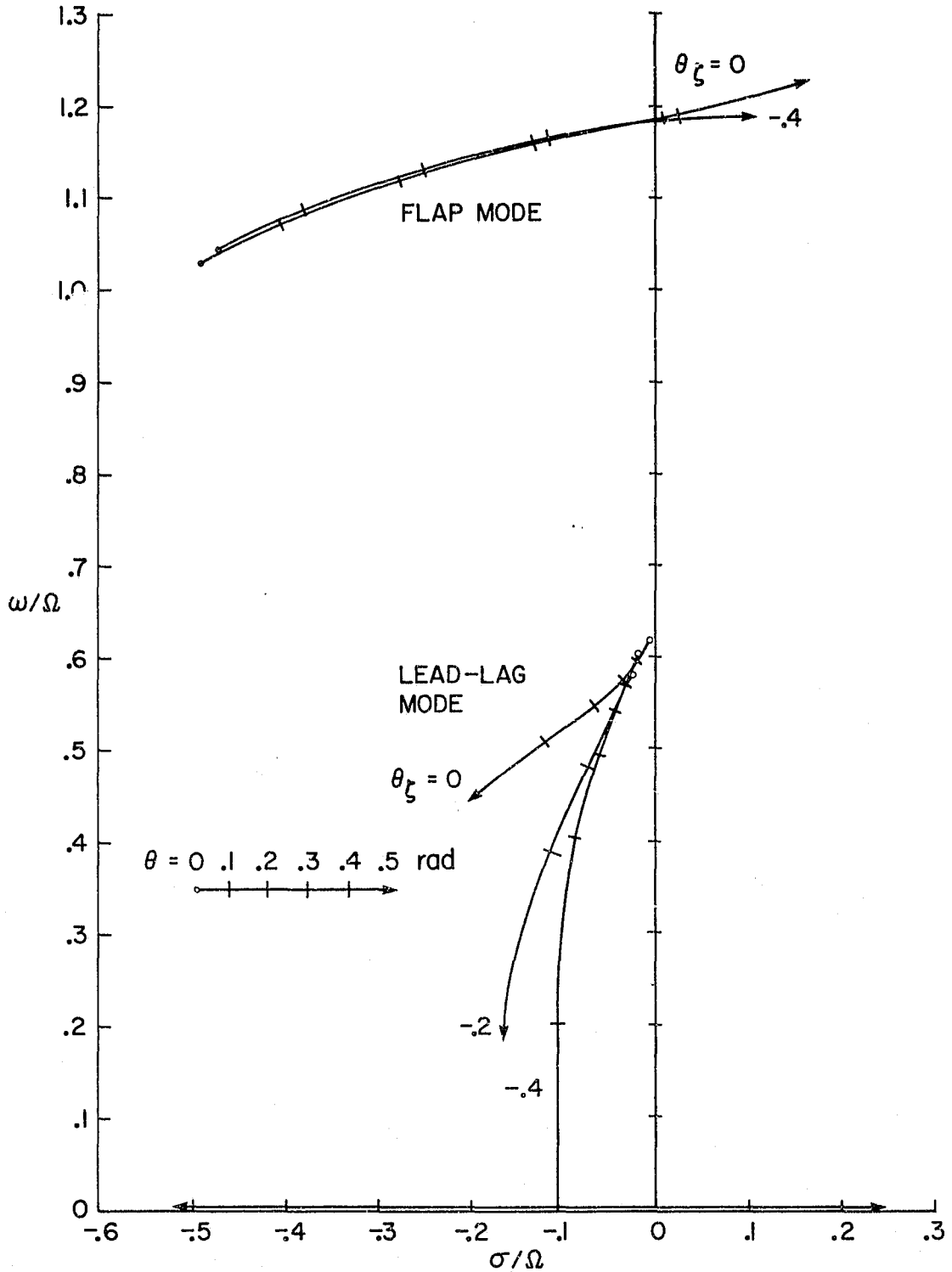

Figure 19. Effect of stall on flap-lag locus of roots with pitch-lag coupling, and principal flexural axis inclination, p = 1.1, $\bar{\omega}_\zeta$ = 0.7, γ = 8, θ_{s_o} = 36°, R = 1.0.

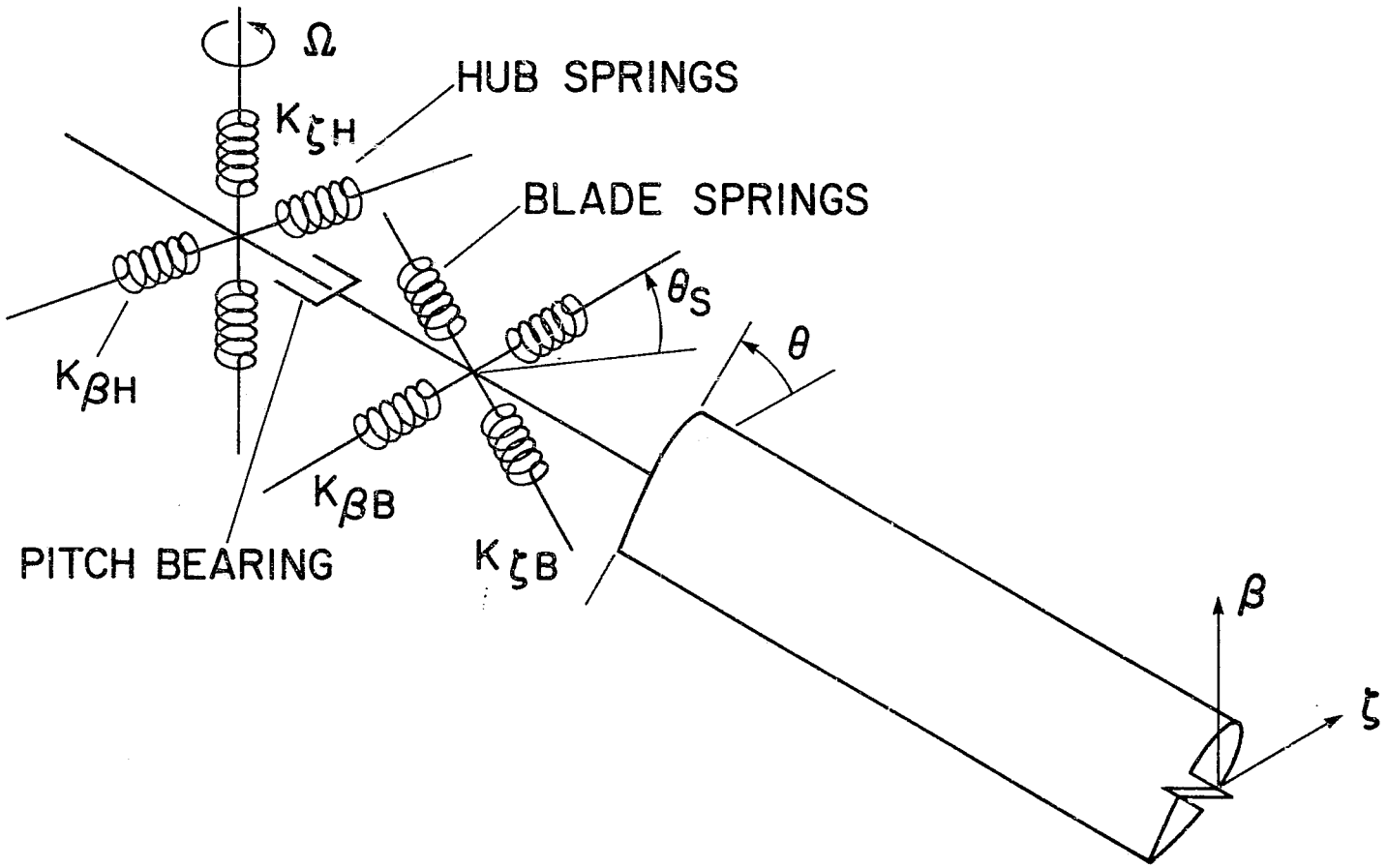

Figure 20. Arrangement of hub and blade flap-lag hinge restraint springs with orientation of blade pitch angle and blade principal flexural (blade spring) axis inclination.